Introduction

The post-ischemic inflammation incites stroke evolution [15, 16, 19–21, 32]. An ischemic insult triggers leukocytes infiltration and astrocyte and microglia activations in the affected brain, leading to the increase of the high-mobility group box1 (HMGB1) in the plasma and brain of the stroke model [19, 21]. The HMGB1 is a potent proinflammatory cytokine secreted by blood-immune [23, 29, 45] and brain-glial cells [35]. This extracellular HMGB1 further activates monocytes/macrophages [3, 34], neutrophils [1, 34], microvascular endothelial cells [12], astrocytes [36] and microglia [24], amplifies the systemic and brain inflammation, and extends the ischemic brain damage into the penumbra [19, 21, 24, 27, 33, 38].

Within the ischemic brain vasculature after middle cerebral artery occlusion (MCAO), circulating platelets [2, 28] and leukocytes [9, 28, 31] are activated, inducing microvascular obstructions and inflammation. In the initial activations of platelet and leukocyte on ischemic endothelium, a large multimeric adhesive glycoprotein von Willebrand factor (VWF) plays a central role. The VWF multimer tethers platelets on the vascular endothelial surface, leading to platelet activation [40]. This platelet-decorated VWF multimer string bound to endothelium supports leukocytes tethering, rolling and transmigration on stimulated vascular endothelial cells, and links thrombosis to inflammation [5, 7, 37]. The platelet binding affinity of VWF increases with increasing length of the VWF multimer strand and with high fluid shear stress [40, 44]. Accordingly, the longest multimer termed ultra-large VWF (ULVWF; secreted by vascular endothelium upon stimulation) exerts its maximum prothrombotic and pro-inflammatory functions in the microvasculture or stenotic vessels under high shear stress condition [30, 40, 41, 43].

A disintegrin and metalloproteinase with thrombospondin type-1 motifs 13 (ADAMTS13) inhibits these VWF functions by cleaving the Tyr1605–Met1606 bond in the A2 domain of the VWF [13, 41]. Physiologically, circulating ADAMTS13 cleaves the ULVWF secreted from endothelial cells, releasing tethered platelets and VWF fragments [11]. In a setting of on-going thrombus formation, the high shear stress induced at the stenotic vasculature stretches plasma-derived VWF multimers (smaller than ULVWF) on the thrombus surface. The extended VWF multimers involved in the platelet thrombosis are consequently cleaved by ADAMTS13 [41]. Notably, by decreasing the interaction between the ULVWF–platelet strands and leukocytes, ADAMTS13 reduces leukocytes adhesion and extravasation on the stimulated vascular wall and down-regulates tissue inflammation [5, 7, 37]. ADAMTS13 deficiency in humans increases the circulating ULVWF resulting in thrombotic thrombocytopenic purpura (TTP) [17, 41]. The TTP manifests fever and neurological deficits associated with VWF–platelet microthrombus formation in the brain. This implies that ADAMTS13 plays a role in inflammation after brain ischemia in TTP patients.

Early studies have shown that ADAMTS13 deficiency aggravates ischemic brain damage in experimental stroke models [14, 48]. We revealed that in the ADAMTS13-deficient mice after a brief focal ischemia the post-ischemic hypoperfusion was significantly amplified partly because of enhanced microvascular plugging by VWF–platelet–leukocyte complex [14]. However, it still remains unclear if an enhanced inflammatory reaction is involved in the deterioration of ischemic brain injury under ADAMTS13 deficiency. Here, we investigated whether ADAMTS13 gene deletion intensifies the increase of extracellular HMGB1, a hallmark of post-stroke inflammation, and exacerbates the brain damage after ischemia–reperfusion.

Materials and methods

Animals

The effect of ADAMTS13 gene deletion on inflammation after brain ischemia was investigated using male ADAMTS13KO and littermate WT mice in an SV129 genetic background, originally generated as a TTP model by our study group [4]. Studies using KO ($n = 31$) and WT ($n = 31$) mice (8–10 weeks of age, 20–23 g of body weight) were approved by the institutional ethics committee. The genotype of each animal was kept unspecified until all experiment's completion.

Middle cerebral artery occlusion

Thirty-minute MCAO by thread insertion from the common carotid artery was induced in KO ($n = 21$) and WT ($n = 21$) mice as previously described [14, 19–21]. Mice were anesthetized with 2% halothane for induction and maintained on 1% halothane in 70% N_2O and 30% O_2 by face mask. Body temperature was maintained at 36.5–37.0°C during surgery. Successful left MCAO was confirmed according to the following criteria: (1) rCBF in the left cerebral cortex at the thread insertion less than 20% of the pre-MCAO rCBF, and (2) consistent presence of significant ischemic neurological symptoms of the left cerebral hemisphere, characterized by right paresis and right circling behavior, during 30-min MCAO. The MCAO surgery was performed within 7 min without bleeding. The anesthesia was discontinued during 30-min MCAO. There were no statistically significant differences in body temperature between the two groups immediately before or after the thread insertion, or 10, 20, and 30 min after

MCAO. The thread was removed under re-anesthesia after 30-min MCAO. Sham surgery in KO ($n = 10$) and WT ($n = 10$) involved temporary insertion (1 s) of the thread into the left common carotid artery without MCAO. There were no statistical differences in prothrombin time or survival rate between KO and WT mice at 24 h after MCAO (Table 1).

Regional cerebral blood flow

The rCBF was measured by laser Doppler flowmetry (LDF) (ALF21, Advance Co., Tokyo, Japan) as previously described [14, 20]. The LDF probe was placed through a guide cannula into the left cerebral cortex stereotaxically (0.22 mm posterior and 2.5 mm lateral from bregma; 1.5 mm depth from the skull surface) on a stereotaxic instrument (Narishige Scientific Instrument Lab: SR-5 M, Tokyo) under anesthesia (pentobarbital 50 mg/kg, i.p.) 24 h before MCAO or sham surgery. The rCBF was monitored in all animals continuously from 30 min before MCAO until immediately after reperfusion. In randomly selected animals, the rCBF was repeatedly recorded over time within 24 h after MCAO. The rCBF during occlusion and reperfusion was expressed as percentages of the preMCAO LDF baseline value.

Infarct volume and neurological deficit

The brains were sectioned coronally (four 2-mm thick slices) according to a mouse brain matrix 24 h after MCAO (KO, $n = 14$ and WT, $n = 15$) or sham operation (KO, $n = 5$ and WT, $n = 5$). The infarct area was measured in each slice stained with 2,3,5 triphenyltetrazolium chloride with an image analysis system (NIH Image, version 1.63), and the infarct volume was calculated [14, 19–21]. Neurological deficit score ranging from 0 (normal motor function) to 5 (no spontaneous motor activity) was measured at 24 h after MCAO [14, 19, 21] (Table 1).

Plasma HMGB1 measurement

The plasma HMGB1 protein was evaluated by western blot 24 h after MCAO. Plasma samples were fractionated by sodium dodecyl sulfate (SDS)-polyacrylamide gel electrophoresis, and HMGB1 levels were determined by immunoblotting with respect to a standard curve, with recombinant HMGB1 as a reference (Sigma-Aldrich, Tokyo) [19, 21]. A blood sample (500 μL) was taken from each experimental animal via inferior vena cava 24 h after MCAO (KO, $n = 11$ and WT, $n = 12$) or sham surgery (KO, $n = 10$ and WT, $n = 10$). The sample was centrifuged (3,000 rpm at 4°C for 10 min), and the supernatant (200 μL) was further centrifuged (15,000 rpm at 4°C for 20 min). SDS sample buffer [125 mmol/L Tris (pH 6.8), 2% SDS, 20% glycerol, 0.0001% bromophenol blue, and 10% β-mercaptoethanol] (100 μL) was added to the plasma extract solution (100 μL), and the resultant sample was heated at 95°C for 5 min. Protein (15 μg) was separated by SDS–polyacrylamide gel electrophoresis (20% gel). Blotting was performed at 2 mA/cm^2 by semi-dry type blotting (Bio-Rad, Tokyo, Japan). The blots were blocked with 5% non-fat dry milk in Tris-buffered saline in 0.1% Tween 20 (TBS-T) at 4°C and incubated with goat polyclonal anti-HMGB1 primary antibody (1:200) (Santa Cruz Biotechnology, Santa Cruz, CA, USA) in TBS-T, followed by bovine anti-goat IgG (heavy chain and light chain [H + L]) alkaline phosphatase conjugate (1:1000) in TBS-T. The blots were visualized with the use of alkaline phosphatase color reagents. The signal intensity of the blots was measured with an image analysis system (NIH Image, version 1.63).

Double immunohistochemical staining for HMGB1/NeuN and HMGB1/MPO

Double immunofluorescent labeling for HMGB1 with NeuN or MPO on paraffin-embedded 5-μm coronal sections

Table 1 Effect of ADAMTS13 gene deletion on brain ischemia in mice after 30-min MCAO and 23.5-h reperfusion

	WT		KO
Brain infarct volume (mm^3)	12.0 ± 2.0 ($n = 15$)	$p < 0.05$[a]	28.5 ± 5.8 ($n = 14$)
Neurological deficit score	1.3 ± 0.2 ($n = 15$)	$p < 0.05$[a]	1.9 ± 0.2 ($n = 14$)
Prothrombin time (s)	12.1 ± 0.8 ($n = 7$)	ns	11.6 ± 0.9 ($n = 6$)
Survival rate (%)	95.2 ($n = 20/21$)	ns	90.4 ($n = 19/21$)

The values are expressed as the mean ± SEM. Neurological deficit score, score 0; normal motor function, 1; flexion of torso and of contralateral forelimb upon lifting of the animal by the tail, 2; circling to the ipsilateral side but normal posture at rest, 3; circling to the ipsilateral side, 4; rolling to the ipsilateral side, 5; leaning to the ipsilateral side at rest (no spontaneous motor activity)

ns Statistically not significant

[a] Student *t* test

of the mouse brain was analyzed by fluorescence microscopy (Nikon, AZ-FL, Tokyo, Japan). At 24 h after MCAO (KO, $n = 5$; WT, $n = 5$) or sham surgery (KO, $n = 5$; WT, $n = 5$), mice were humanely perfused transcardially with saline and 4% paraformaldehyde. The brains were removed of fat and water using an autodegreasing unit (RH-12; Sakura Seiko Co, Tokyo) and embedded in paraffin. Subsequently, 5-μm sections were mounted on slides and dried at 37°C for 1 day. After deparaffinization and rehydration, the sections were incubated with primary antibodies of biotinylated anti-mouse NeuN (1:200; Chemicon International, Temecula, CA, USA) or rabbit polyclonal anti-MPO (1:200; DAKO Inc., Carpinteria, CA, USA) and of goat polyclonal anti-HMGB1 (1:200; Santa Cruz Biotechnology, Santa Cruz, CA, USA) overnight at 4°C. Sections were then incubated with donkey anti-goat IgG-FITC secondary antibody (1:200; Santa Cruz Biotechnology) for 1 h, and thereafter with goat anti-rabbit IgG-Texas red secondary antibody (1:200; Santa Cruz Biotechnology) or Ultra avidine Texas Red (1:200; Leinco Technologies) for 1 h. The sections were imaged and analyzed. The histological findings were evaluated by neuropathologists until a consensus was obtained. The fluorescence intensity (for cells positive to NeuN, MPO, or HMGB1) in five randomly selected areas (150 μm × 200 μm for each) from the region of interest in the ischemic cerebral cortex (as indicated in Figs. 2, 3) was evaluated with an image analysis system (NIH Image, version 1.63) with the corresponding non-ischemic contralateral regions as a control, and the relative fluorescence intensity was calculated. In ischemic stroke, the necrotic core is surrounded by a zone of reactive/inflammatory cytosis which can extend the initial insult into the penumbra with delayed cell death. Based on this concept, the region of interest in the cortical penumbra for the fluorescence evaluation was decided as indicated.

Statistical analysis

Data are presented as mean ± standard error of mean (SEM). For multiple pairwise comparisons in parametric analysis, two-way analysis of variance (ANOVA) followed by Tukey–Kramer's test was performed. When only two groups were compared, Student's *t* test was used. Probability values of <0.05 were considered statistically significant.

Results

Brain infarction

The ADAMTS13 gene knockout (ADAMTS13KO) mice group had a significantly larger volume of brain infarction compared with the wild-type (WT) following 23.5-h reperfusion after 30-min MCAO (Student's *t* test) (Table 1). No ischemic brain damage was observed in either KO or WT mice after sham operation.

Neurological deficits

ADAMTS13KO mice had more severe neurological deficits than the WT (Student's *t* test) 24 h after MCAO (Table 1).

Regional cerebral blood flow

The rCBF showed no statistical differences between the two groups during MCAO or immediately after reperfusion. However, the rCBF in ADAMTS13KO mice progressively decreased significantly more markedly compared to WT during the first 30-min reperfusion (Tukey–Kramer's test). 24 h after MCAO, the rCBF in KO mice remained significantly lower compared to WT (Student's *t* test) (Table 2).

ADAMTS13 gene deletion enhances post-ischemic increase of plasma HMGB1

A 30-min MCAO and 23.5-h reperfusion significantly increased the plasma HMGB1 level both in ADAMTS13KO and WT mice as compared to sham operation (Fig. 1). However, this increase of plasma HMGB1 after MCAO was more markedly enhanced in ADAMTS13KO mice than in WT (Tukey–Kramer's test).

ADAMTS13 gene deletion intensifies post-ischemic brain inflammation and neuronal death

Double immunohistochemical staining for HMGB1/NeuN and HMGB1/MPO

The qualitative analysis of double immunofluorescent labeling for HMGB1 with NeuN (neuron-specific nuclear protein) or MPO (myeloperoxidase) on the cortical tissue 24 h after MCAO or sham operation showed that (1) the number of neurons immunoreactive to NeuN in the ischemic penumbra decreased more in ADAMTS13KO mice compared to WT (Fig. 2), (2) HMGB1 immunoreactivity disappeared in the ischemic neuronal nuclei in both KO and WT mice, suggestive of a translocation of HMGB1 from neuronal nucleus either to neuronal cytoplasm or to extracellular space (Fig. 2), and (3) cells with co-expression of MPO (a marker for neutrophils, macrophages and/or microglia) and HMGB1 appeared more prominently in the ischemic penumbra in ADAMTS13KO mice than in WT (Fig. 3).

Table 2 Effect of ADAMTS13 gene deletion on regional cerebral blood flow (rCBF) in mice of 30-min MCAO model

	WT ($n = 6$)		KO ($n = 7$)
Time (min)			
Baseline	100.0 ± 0	ns	100.0 ± 0
0	13.6 ± 4.6	ns	13.2 ± 2.0
10	17.9 ± 3.4	ns	22.4 ± 6.3
20	17.7 ± 5.2	ns	19.3 ± 5.7
30	16.8 ± 4.7	ns	18.6 ± 3.5
Reperfusion	114.3 ± 19.1	ns	88.1 ± 8.1
40	90.5 ± 12.7	$p < 0.05$[a]	48.4 ± 8.4
50	93.8 ± 11.3	$p < 0.01$[a]	35.4 ± 7.7
60	83.2 ± 6.8	$p < 0.01$[a]	28.1 ± 4.7
Time (hour)			
24	72.9 ± 13.9	$p < 0.05$[b]	37.2 ± 5.9

rCBF values are expressed as the mean ± SEM (% of baseline)

[a] Turkey-Kramer's test after two-way repeated measures ANOVA [$F(8,98) = 5.841$, $p < 0.0001$)]

[b] Student's t test

Relative fluorescent intensity of NeuN, MPO and HMGB1

The relative fluorescent intensity (%) in the ischemic cerebral cortex 24 h after MCAO was significantly decreased for NeuN in ADAMTS13KO mice compared to WT [57.5 ± 8.7 in KO vs. 93.2 ± 5.5 in WT ($p < 0.05$, student's t test)], and increased for both MPO and HMGB1 more in ADAMTS13KO mice than in WT [KO vs. WT: 557.7 ± 139.8 vs. 310.4 ± 131.7 for MPO, and 159.7 ± 46.5 vs. 70.2 ± 35.1 for HMGB1 (although not statistically significant)].

Discussion

The (UL)VWF, the substrate of ADAMTS13, recruits platelets and leukocytes onto the injured vascular endothelium, and mediates microvascular plugging and enhances the tissue inflammation [5, 7, 30, 37, 40, 41, 43, 44]. ADAMTS13 inhibits these prothrombotic and proinflammatory functions of (UL)VWF [7, 13, 41]. Our current study implies that ADAMTS13 gene deletion amplifies systemic and brain inflammatory responses against brain ischemia–reperfusion enhancing a potent cytokine HMGB1 neurotoxicity, leads to progressive decline of post-ischemic cerebral blood reflow, and exacerbates ischemic brain injury. ADAMTS13 may play a neuroprotective role against inflammation in ischemic stroke.

ADAMTS13 deficiency may promote inflammation by activating platelets, leukocytes, and vascular endothelium after brain ischemia–reperfusion. Responding to ischemia–

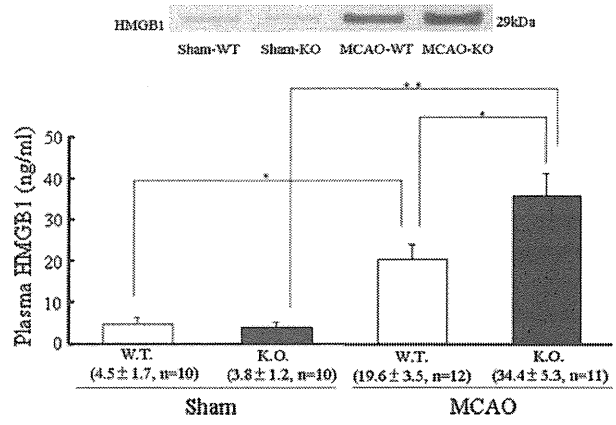

Fig. 1 Effect of ADAMTS13 gene deletion on plasma HMGB1 in mice after 30-min MCAO. The plasma HMGB1 protein was evaluated by western blot. Transient focal ischemia of 30-min MCAO followed by 23.5-h reperfusion significantly increased the plasma HMGB1 level both in ADAMTS13KO and WT mice when compared to sham operation [plasma HMGB1 (ng/ml): MCAO-KO; 34.4 ± 5.3 vs. sham-KO; 3.8 ± 1.2, $p < 0.01$, and MCAO-WT; 19.6 ± 3.5 vs. sham-WT; 4.5 ± 1.7, $p < 0.05$, Tukey–Kramer's test after two-way ANOVA ($F(1,40) = 38.401$, $p < 0.01$)]. This increase of plasma HMGB1 at 24 h after MCAO was more markedly enhanced in ADAMTS13KO mice than in WT [MCAO-KO; 34.4 ± 5.3 vs. MCAO-WT; 19.6 ± 3.5, $p < 0.05$, Tukey–Kramer's test after two-way ANOVA ($F(1,40) = 4.296$, $p < 0.05$)]. Sham-WT $n = 10$, Sham-KO $n = 10$, MCAO-WT $n = 12$, MCAO-KO $n = 11$. Values are expressed as the mean ± SEM. $*p < 0.05$, $**p < 0.01$, Tukey–Kramer's test after two-way ANOVA

reperfusion, the stimulated vascular endothelial cells secrete ULVWF [44]. Binding of VWF to the platelet membrane glycoprotein initiates a signaling cascade that causes platelet activation [25, 46]. The activated platelets release multiple proinflammatory factors, mitogenic mediators, metalloproteinases, and reactive oxygen species, and stimulate the leukocytes and endothelium to incite inflammatory reactions [8, 10]. Further, the platelet–(UL)VWF string directly supports the leukocyte transmigration into the inflammatory tissue [5, 7, 37]. Thus, the VWF-cleaving protease ADAMTS13 plays a role as an anti-inflammatory factor, and therefore its deficiency can exaggerate the post-ischemic inflammation.

In ADAMTS13KO mice after a cerebral ischemia, the plasma HMGB1 increased more and the HMGB1-expressing immune cells appeared more prominent in the cortical penumbra than in WT. The increased extracellular HMGB1 may contribute to secondary ischemic brain damage in ADAMTS13KO mice. The HMGB1, a DNA-binding protein, is a central proinflammatory cytokine [29]. Upon inflammatory signals, the chromosomal HMGB1 relocates into cytoplasmic secretory lysosomes and is secreted into the immunological synapse [29] or into the extracellular space by monocytes/macrophages [45], neutrophils [23], mature dendritic cells [29], natural killer cells

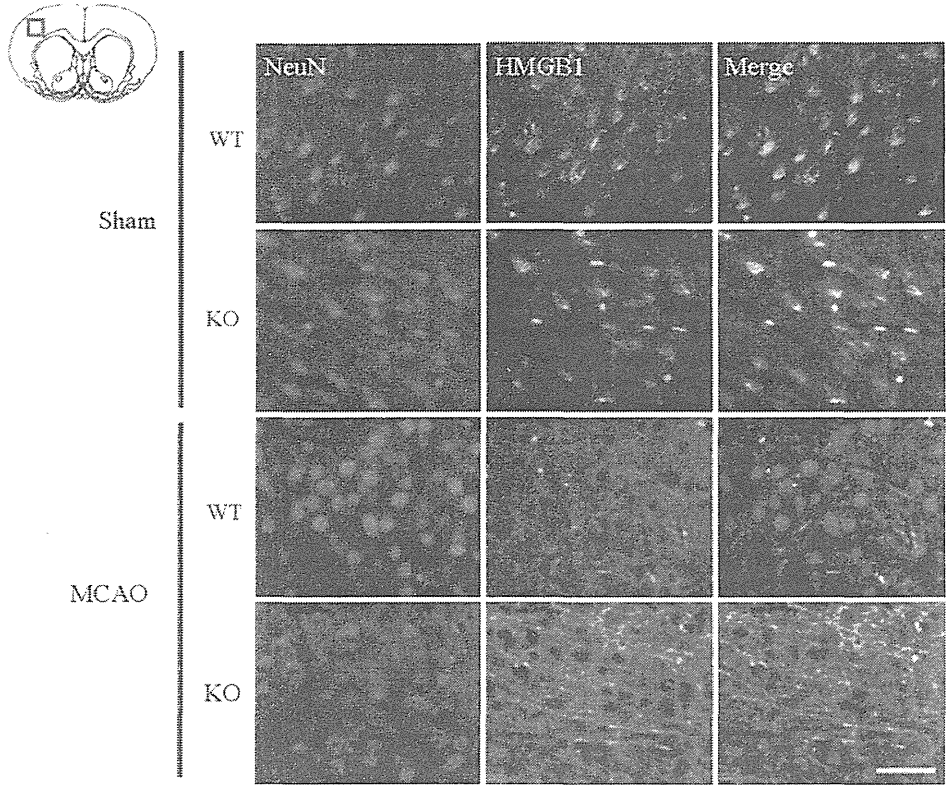

Fig. 2 Effect of ADAMTS13 gene deletion on NeuN positive cells expressing HMGB1 in mice brain after 30-min MCAO. Qualitative analysis of double immunofluorescent labeling for HMGB1 with NeuN on the brain tissue 24 h after MCAO showed that the number of neurons immunoreactive to NeuN in the ischemic cortical penumbra decreased more in ADAMTS13KO mice than WT. The HMGB1 immunoreactivity disappeared in the ischemic neuronal nuclei in both KO and WT mice, suggesting that neuronal-nuclear HMGB1 translocated into either the neuronal cytoplasm or the extracellular space. In addition, the HMGB1 immunoreactivity seemed to increase in the ischemic cortical tissue in the ADAMTS13KO mice, indicating a possibility that non-neuronal HMGB1 positive cells were activated in the KO mice compared to the WT ($n = 5$ in each group). *Scale bar* 50 μm. NeuN positive cells *red*, HMGB1 positive cells *green*, merge *yellow*

[29], and glia [35]. HMGB1 also leaks from necrotic cells [42] and ischemic neurons [38]. The extracellular HMGB1 binds to its receptors, RAGE (receptor for advanced glycation end products) [22], Toll-like receptor 2 (TLR2), and TLR4 [34], recapitulates the intracellular signaling cascades initiated by early proinflammatory stresses, and thus propagates continuous proinflammatory responses [3, 22, 29, 34, 42]. Naturally, high blood HMGB1 correlates with the severity of systemic inflammation [29, 45].

After brain ischemia, extracellular HMGB1 increases rapidly in the blood and central nervous system, and induces neuroinflammation [24, 38]. HMGB-1 early released from the striatal ischemic core can bind to RAGE that is robustly expressed in the peri-infarct region, and extend the ischemic brain injury [38]. HMGB1-RAGE signaling in infiltrating macrophages and activated microglia seemingly mediate neuronal death evolution in the ischemic penumbra [33]. The HMGB1 inhibition in the brain or systemic circulation protects the blood–brain barrier and the brain from ischemia [24, 27, 33, 47]. Inhibition of leukocytes and microglia results in decreased HMGB1 levels in the brain and plasma, reduces apoptosis in the ischemic brain, and improves brain atrophy and neurologic deficits [19, 21]. Therefore, the increased extracellular HMGB1 in the blood and brain of ADAMTS13KO mice as observed in our study can exacerbate ischemic brain injury by intensifying systemic and brain inflammation. Interestingly, the platelet intracellular HMGB1 is exported to the external surface of the plasma membrane upon its activation [39]. Accordingly, the activated platelet may be an additional source of the exceedingly increased plasma HMGB1 in ADAMTS13KO mice after brain ischemia, where enhanced VWF–platelet interactions develop [14]. We suggest that ADAMTS13 deficiency multiplies secondary insults after brain ischemia by up-regulating (UL)VWF-mediating inflammation and enhancing HMGB1 neurotoxicity in the systemic and local environments.

This study suggests a potential therapy with ADAMTS13 for acute ischemic stroke by breaking a vicious circle

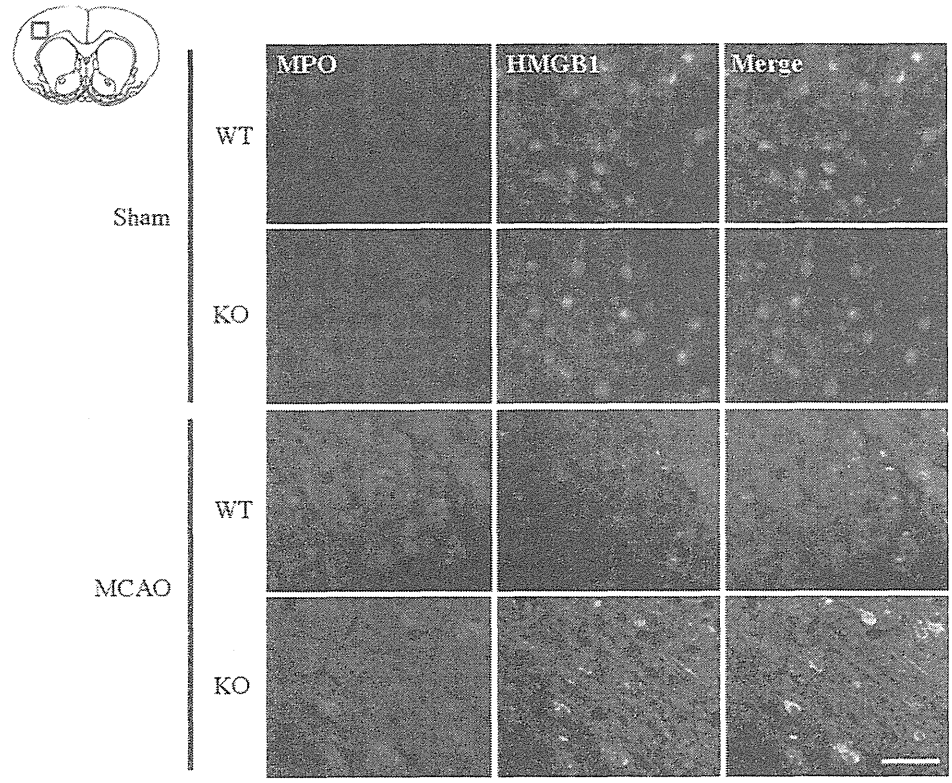

Fig. 3 Effect of ADAMTS13 gene deletion on MPO positive cells expressing HMGB1 in mice brain after 30-min MCAO. Qualitative analysis of double immunofluorescent labeling for HMGB1 with MPO on the brain tissue 24 h after MCAO showed that cells co-expressing MPO and HMGB1 were more prominent in the ischemic cortical penumbra in KO mice than in WT ($n = 5$ in each group). *Scale bar* 50 μm. MPO positive cells *red*, HMGB1 positive cells *green*, merge *yellow*

of thrombosis and inflammation. The (UL)VWF–platelet string interacts with leukocytes, and provokes inflammation [5, 7, 37]. The inflammation induces the endothelial-ULVWF secretion [44]. The proinflammatory cytokines from leukocytes and endothelial cells [such as tumor necrosis factor (TNF)-α and interleukin (IL)-8] stimulate the endothelial ULVWF release and IL-6 protects the ULVWF from cleavage [6]. This would increase the number of ULVWF multimers in plasma sufficiently to aggregate platelets and on vascular endothelial surface to tether platelets and leukocytes onto the endothelium, providing a linkage between thrombosis and inflammation. Of note, HMGB1 stimulates the monocytes/macrophages [3, 34], neutrophils [1, 34] and glial cells [24, 36, 38] to produce TNF-α, IL-1, IL-6 and/or IL-8, and incites the microvascular endothelial cells [12, 38] to express TNF-α, IL-8 and various adhesion molecules. Namely, the increased plasma HMGB1 in ADAMTS13-deficient mice can upregulate ULVWF, and thus reinforce the association between inflammation and thrombosis. ADAMTS13 may prevent stroke evolution by interfering with the crosstalk between thrombosis and inflammation.

Thrombolytic therapy using tissue plasminogen activator (tPA) for acute stroke has limitations in the therapeutic time window and in the drug dosage due to the risk of hemorrhagic transformation [18]. Further, tPA directly exerts neurotoxicity in the ischemic brain [26]. We suggest that a regulation of the interaction between (UL)VWF–platelet and leukocyte using ADAMTS13 may become a novel therapeutic option in acute brain ischemia. ADAMTS13 does not dissolve the VWF–platelet–primary hemostatic thrombus in the absence of pathologically high fluid shear stress. Therefore, ADAMTS13 may be particularly well suited for acute ischemic stroke without increasing hemorrhagic complications. An early experimental study [48] together with our preliminary data (not shown) demonstrated that recombinant human ADAMTS13 administration reduced infarct volume in stroke model in a VWF-dependent manner without producing cerebral hemorrhage.

This study has several limitations. For example, the reduction of cerebral blood reflow in ADAMTS13KO mice after ischemic insult was continuous and higher than that observed in WT. Therefore, even without the amplified inflammation with HMGB1 neurotoxic effects, only the difference in the blood flow recovery might explain the following more deleterious events in the ischemic brain of ADAMTS13-deficient mice compared to WT. The enhanced elevation of the plasma HMGB1 under ADAMTS13 deficiency after brain ischemia might be also explained simply by the more exacerbated brain damage, regardless of the theoretically intensified interactions between the platelet–(UL)VWF strands and the leukocytes without VWF cleaving protease. The future study required to clarify these issues would include chronological data

evaluations in the stroke experiments with permanent ischemic procedure (deleting the reperfusion effect) or with enhancing/inhibiting HMGB1 activities by drugs or genetic manipulations.

Conclusions

A gene deletion of ADAMTS13 renders mice more vulnerable to brain ischemia–reperfusion injury than their wild-type counterparts, when subjected to 30-min MCAO. This preliminary study suggests that ADAMTS13 deficiency may exacerbate systemic and neuronal inflammation after brain ischemia via VWF-dependent pathway, although this remains still hypothetical. Further studies are warranted to better characterize the role of ADAMTS13 in brain ischemia–reperfusion and to provide a novel therapeutic approach for ischemic stroke by regulating VWF-dependent inflammation as well as microvascular plugging.

References

1. Abraham E, Arcaroli J, Carmody A, Wang H, Tracey KJ (2000) HMG-1 as a mediator of acute lung inflammation. J Immunol 165:2950–2954
2. Abumiya T, Fitridge R, Mazur C, Copeland BR, Koziol JA, Tschopp JF, Pierschbacher MD, del Zoppo GJ (2000) Integrin alpha(IIb)beta(3) inhibitor preserves microvascular patency in experimental acute focal cerebral ischemia. Stroke 31:1402–1409
3. Andersson U, Wang H, Palmblad K, Aveberger AC, Bloom O, Erlandsson-Harris H, Janson A, Kokkola R, Zhang M, Yang H, Tracey KJ (2000) High mobility group 1 protein (HMG-1) stimulates proinflammatory cytokine synthesis in human monocytes. J Exp Med 192:565–570
4. Banno F, Kokame K, Okuda T, Honda S, Miyata S, Kato H, Tomiyama Y, Miyata T (2006) Complete deficiency in ADAMTS13 is prothrombotic, but it alone is not sufficient to cause thrombotic thrombocytopenic purpura. Blood 107:3161–3166
5. Bernardo A, Ball C, Nolasco L, Choi H, Moake JL, Dong JF (2005) Platelets adhered to endothelial cell-bound ultra-large von Willebrand factor strings support leukocyte tethering and rolling under high shear stress. J Thromb Haemost 3:562–570
6. Bernardo A, Ball C, Nolasco L, Moake JF, Dong JF (2004) Effects of inflammatory cytokines on the release and cleavage of the endothelial cell-derived ultralarge von Willebrand factor multimers under flow. Blood 104:100–106
7. Chauhan AK, Kisucka J, Brill A, Walsh MT, Scheiflinger F, Wagner DD (2008) ADAMTS13: a new link between thrombosis and inflammation. J Exp Med 205:2065–2074
8. Davi G, Patrono C (2007) Platelet activation and atherothrombosis. N Engl J Med 357:2482–2494
9. Del Zoppo GJ, Schmid-Schonbein GW, Mori E, Copeland BR, Chang CM (1991) Polymorphonuclear leukocytes occlude capillaries following middle cerebral artery occlusion and reperfusion in baboons. Stroke 22:1276–1283
10. Dole VS, Bergmeier W, Mitchell HA, Eichenberger SC, Wagner DD (2005) Activated platelets induce Weibel-Palade-body secretion and leukocyte rolling in vivo: role of P-selectin. Blood 106: 2334–2339
11. Dong JF, Moake JL, Nolasco L, Bernardo A, Arceneaux W, Shrimpton CN, Schade AJ, McIntire LV, Fujikawa K, López JA (2002) ADAMTS-13 rapidly cleaves newly secreted ultralarge von Willebrand factor multimers on the endothelial surface under flowing conditions. Blood 100:4033–4039
12. Fiuza C, Bustin M, Talwar S, Tropea M, Gerstenberger E, Shelhamer JH, Suffredini AF (2003) Inflammation-promoting activity of HMGB1 on human microvascular endothelial cells. Blood 101:2652–2660
13. Fujikawa K, Suzuki H, McMullen B, Chung DP (2001) Purification of human von Willebrand factor-cleaving protease and its identification as a new member of the metalloproteinase family. Blood 98:1662–1666
14. Fujioka M, Hayakawa K, Mishima K, Kunizawa A, Irie K, Higuchi S, Nakano T, Muroi C, Fukushima H, Sugimoto M, Banno F, Kokame K, Miyata T, Fujiwara M, Okuchi K, Nishio K (2010) ADAMTS13 gene deletion aggravates ischemic brain damage: a possible neuroprotective role of ADAMTS13 by ameliorating postischemic hypoperfusion. Blood 115:1650–1653
15. Fujioka M, Taoka T, Matsuo Y, Hiramatsu KI, Sakaki T (1999) Novel brain ischemic change on MRI. Delayed ischemic hyperintensity on T1-weighted images and selective neuronal death in the caudoputamen of rats after brief focal ischemia. Stroke 30:1043–1046
16. Fujioka M, Taoka T, Matsuo Y, Mishima K, Ogoshi K, Kondo Y, Tsuda M, Fujiwara M, Asano T, Sakaki T, Miyasaki A, Park D, Siesjö BK (2003) Magnetic resonance imaging shows delayed ischemic striatal neurodegeneration. Ann Neurol 54:732–747
17. Furlan M, Robles R, Galbusera M, Remuzzi G, Kyrle PA, Brenner B, Krause M, Scharrer I, Aumann V, Mittler U, Solenthaler M, Lammle B (1998) von Willebrand factor-cleaving protease in thrombotic thrombocytopenic purpura and the hemolytic-uremic syndrome. N Engl J Med 339:1578–1584
18. Hacke W, Kaste M, Bluhmki E, Brozman M, Davalos A, Guidetti D, Larrue V, Lees KR, Medeghri Z, Machnig T, Schneider D, von Kummer R, Wahlgren N, Toni D (2008) Thrombolysis with alteplase 3 to 4.5 hours after acute ischemic stroke. N Engl J Med 359: 1317–1329
19. Hayakawa K, Mishima K, Irie K, Hazekawa M, Mishima S, Fujioka M, Orito K, Egashira N, Katsurabayashi S, Takasaki K, Iwasaki K, Fujiwara M (2008) Cannabidiol prevents a post-ischemic injury progressively induced by cerebral ischemia via a high-mobility group box1-inhibiting mechanism. Neuropharmacology 55:1280–1286
20. Hayakawa K, Mishima K, Nozako M, Hazekawa M, Irie K, Fujioka M, Orito K, Abe K, Hasebe N, Egashira N, Iwasaki K, Fujiwara M (2007) Delayed treatment with cannabidiol has a cerebroprotective action via a cannabinoid receptor-independent myeloperoxidase-inhibiting mechanism. J Neurochem 102:1488–1496
21. Hayakawa K, Mishima K, Nozako M, Hazekawa M, Mishima S, Fujioka M, Orito K, Egashira N, Iwasaki K, Fujiwara M (2008) Delayed treatment with minocycline ameliorates neurologic impairment through activated microglia expressing a high-mobility group box1-inhibiting mechanism. Stroke 39:951–958
22. Hori O, Brett J, Slattery T, Cao R, Zhang J, Chen JX, Nagashima M, Lundh ER, Vijay S, Nitecki D et al (1995) The receptor for advanced glycation end products (RAGE) is a cellular binding site for amphoterin. Mediation of neurite outgrowth and co-expression of rage and amphoterin in the developing nervous system. J Biol Chem 270:25752–25761
23. Ito İ, Fukazawa J, Yoshida M (2007) Post-translational methylation of high mobility group box 1 (HMGB1) causes its cytoplasmic localization in neutrophils. J Biol Chem 282: 16336–16344

24. Kim JB, Sig Choi J, Yu YM, Nam K, Piao CS, Kim SW, Lee MH, Han PL, Park JS, Lee JK (2006) HMGB1, a novel cytokine-like mediator linking acute neuronal death and delayed neuroinflammation in the postischemic brain. J Neurosci 26:6413–6421
25. Kroll MH, Harris TS, Moake JL, Handin RI, Schafer AI (1991) von Willebrand factor binding to platelet GpIb initiates signals for platelet activation. J Clin Invest 88:1568–1573
26. Liu D, Cheng T, Guo H, Fernandez JA, Griffin JH, Song X, Zlokovic BV (2004) Tissue plasminogen activator neurovascular toxicity is controlled by activated protein C. Nat Med 10: 1379–1383
27. Liu K, Mori S, Takahashi HK, Tomono Y, Wake H, Kanke T, Sato Y, Hiraga N, Adachi N, Yoshino T, Nishibori M (2007) Anti-high mobility group box 1 monoclonal antibody ameliorates brain infarction induced by transient ischemia in rats. FASEB J 21:3904–3916
28. Lo EH, Dalkara T, Moskowitz MA (2003) Mechanisms, challenges and opportunities in stroke. Nat Rev Neurosci 4:399–415
29. Lotze MT, Tracey KJ (2005) High-mobility group box 1 protein (HMGB1): nuclear weapon in the immune arsenal. Nat Rev Immunol 5:331–342
30. Moake JL, Rudy CK, Troll JH, Weinstein MJ, Colannino NM, Azocar J, Seder RH, Hong SL, Deykin D (1982) Unusually large plasma factor VIII: von Willebrand factor multimers in chronic relapsing thrombotic thrombocytopenic purpura. N Engl J Med 307:1432–1435
31. Mori E, del Zoppo GJ, Chambers JD, Copeland BR, Arfors KE (1992) Inhibition of polymorphonuclear leukocyte adherence suppresses no-reflow after focal cerebral ischemia in baboons. Stroke 23:712–718
32. Mori T, Town T, Tan J, Tateishi N, Asano T (2005) Modulation of astrocytic activation by arundic acid (ONO-2506) mitigates detrimental effects of the apolipoprotein E4 isoform after permanent focal ischemia in apolipoprotein E knock-in mice. J Cereb Blood Flow Metab 25:748–762
33. Muhammad S, Barakat W, Stoyanov S, Murikinati S, Yang H, Tracey KJ, Bendszus M, Rossetti G, Nawroth PP, Bierhaus A, Schwaninger M (2008) The HMGB1 receptor RAGE mediates ischemic brain damage. J Neurosci 28:12023–12031
34. Park JS, Svetkauskaite D, He Q, Kim JY, Strassheim D, Ishizaka A, Abraham E (2004) Involvement of toll-like receptors 2 and 4 in cellular activation by high mobility group box 1 protein. J Biol Chem 279:7370–7377
35. Passalacqua M, Patrone M, Picotti GB, Del Rio M, Sparatore B, Melloni E, Pontremoli S (1998) Stimulated astrocytes release high-mobility group 1 protein, an inducer of LAN-5 neuroblastoma cell differentiation. Neuroscience 82:1021–1028
36. Pedrazzi M, Patrone M, Passalacqua M, Ranzato E, Colamassaro D, Sparatore B, Pontremoli S, Melloni E (2007) Selective proinflammatory activation of astrocytes by high-mobility group box 1 protein signaling. J Immunol 179:8525–8532
37. Pendu R, Terraube V, Christophe OD, Gahmberg CG, de Groot PG, Lenting PJ, Denis CV (2006) P-selectin glycoprotein ligand 1 and beta2-integrins cooperate in the adhesion of leukocytes to von Willebrand factor. Blood 108:3746–3752
38. Qiu J, Nishimura M, Wang Y, Sims JR, Qiu S, Savitz SI, Salomone S, Moskowitz MA (2008) Early release of HMGB-1 from neurons after the onset of brain ischemia. J Cereb Blood Flow Metab 28:927–938
39. Rouhiainen A, Imai S, Rauvala H, Parkkinen J (2000) Occurrence of amphoterin (HMG1) as an endogenous protein of human platelets that is exported to the cell surface upon platelet activation. Thromb Haemost 84:1087–1094
40. Ruggeri ZM (2007) The role of von Willebrand factor in thrombus formation. Thromb Res 120(Suppl 1):S5–S9
41. Sadler JE (2008) Von Willebrand factor, ADAMTS13, and thrombotic thrombocytopenic purpura. Blood 112:11–18
42. Scaffidi P, Misteli T, Bianchi ME (2002) Release of chromatin protein HMGB1 by necrotic cells triggers inflammation. Nature 418:191–195
43. Siedlecki CA, Lestini BJ, Kottke-Marchant KK, Eppell SJ, Wilson DL, Marchant RE (1996) Shear-dependent changes in the three-dimensional structure of human von Willebrand factor. Blood 88:2939–2950
44. Vischer UM (2006) von Willebrand factor, endothelial dysfunction, and cardiovascular disease. J Thromb Haemost 4:1186–1193
45. Wang H, Bloom O, Zhang M, Vishnubhakat JM, Ombrellino M, Che J, Frazier A, Yang H, Ivanova S, Borovikova L, Manogue KR, Faist E, Abraham E, Andersson J, Andersson U, Molina PE, Abumrad NN, Sama A, Tracey KJ (1999) HMG-1 as a late mediator of endotoxin lethality in mice. Science 285:248–251
46. Yin H, Liu J, Li Z, Berndt MC, Lowell CA, Du X (2008) Src family tyrosine kinase Lyn mediates VWF/GPIb-IX-induced platelet activation via the cGMP signaling pathway. Blood 112: 1139–1146
47. Zhang J, Takahashi HK, Liu K, Wake H, Liu R, Maruo T, Date I, Yoshino T, Ohtsuka A, Mori S, Nishibori M (2011) Anti-high mobility group box-1 monoclonal antibody protects the blood–brain barrier from ischemia-induced disruption in rats. Stroke 42:1420–1428
48. Zhao BQ, Chauhan AK, Canault M, Patten IS, Yang JJ, Dockal M, Scheiflinger F, Wagner DD (2009) von Willebrand factor-cleaving protease ADAMTS13 reduces ischemic brain injury in experimental stroke. Blood 114:3329–3334

第73回日本血液学会学術集会
シンポジウム6
血栓止血学・血管生物学
の最近の進歩

ADAMTS13研究の最先端

宮田敏行[1]，　小亀浩市[1]，　秋山正志[1]，　坂野史明[1]，
中山大輔[1]，　武田壮一[2]

Key words : ADAMTS13, Platelet, Thrombotic thrombocytopenic purpura, Von Willebrand factor

はじめに
血栓性血小板減少性紫斑病とは

血栓性血小板減少性紫斑病（thrombotic thrombocytopenic purpura, TTP）は微小血管内に血小板血栓が生じる致死率の高い疾患である。TTPは血中のフォンビルブランド因子（VWF）切断酵素であるADAMTS13が先天性もしくは後天性の原因により活性が著減し，超高分子量VWFマルチマーが血中に蓄積し，これが引き金となり血小板血栓が形成される。微小血管に血小板血栓ができるため，消費性に血小板数の減少を示し，赤血球が血栓に衝突し損傷を受けるため，破砕赤血球が見られ溶血性貧血を示す。脳の微小血管が閉塞すると虚血性または梗塞性の障害として動揺する精神・神経症状が観察される。また，長期にわたって腎機能障害がみられる。VWFは2,050アミノ酸残基のモノマーがN末端どうし，C末端どうしでジスルフィド結合を介して直鎖状に繋がり，超高分子量マルチマー（unusually large VWF multimer, UL-VWFマルチマー）として合成され血管内皮細胞から血中に分泌される。このUL-VWFマルチマーは血小板活性化能が高く，これが血中に蓄積するTTP患者では，微小血管に血小板血栓が生じる。このTTPの病態は血漿交換により劇的に改善される。これは血漿交換によりADAMTS13に対する抗体が血漿から除去されること，かつADAMTS13が補充されることによる。これにより，ADAMTS13活性が回復し，超高分子量VWFマルチマーが通常のマルチマーまで分解され，血小板血栓の形成が抑制される[1~4]。

先天性ADAMTS13欠損症の遺伝子解析と
ADAMTS13活性測定基質の開発

TTPの原因遺伝子として，血漿メタロプロテアーゼADAMTS13が2001年にクローニングされた[5~7]。私達は奈良県立医科大学藤村吉博教授と共同研究を行い，まず先天性ADAMTS13欠損症の遺伝子解析を行った。その結果，C908Y変異は本州に，R193W変異は瀬戸内地域と東北地方に，Q449Xは東北地方に複数例みられるなど，変異の地理的な分布も示すことができるまでにADAMTS13の遺伝子変異の情報が蓄積された[8,9]。これらの先天性ADAMTS13欠損症のうち幾人かは，妊娠時に先天性ADAMTS13欠損症によるTTPと診断された[10]。また，脳梗塞治療薬として広く用いられていた抗血小板薬チクロピジンの副作用として，極めて頻度は低いがTTPの発症例が報告された[11]。ADAMTS13活性を簡便に測定できればTTPの診断を早期に行えるが，当時は活性測定にSDS-アガロース・抗VWF抗体ウェスタンブロット法を用いていたので数日を要した。そこで私達はADAMTS13の簡易測定法の開発に着手し，VWFのA2ドメイン内の73残基が最小基質であることを明らかにした[12]。その後，切断部位であるTyr1605-Met1606結合をはさみ蛍光基と消光基を導入した蛍光基質FRETS-VWF73を開発した[13]。本基質は蛍光共鳴エネルギー転移により自家蛍光が抑えられているが，ADAMTS13によりTyr1605-Met1606結合が切断されると蛍光を発する。本基質を用いると30分以内にADAMTS13活性を定量できる。

[1]国立循環器病研究センター　分子病態部
[2]国立循環器病研究センター　心臓生理機能部

日本人一般住民を対象にしたADAMTS13活性測定と先天性ADAMTS13欠損症の推定頻度

簡便で定量性のあるADAMTS13活性測定基質を開発したので，本基質を用いて日本人3,616人（男性1,687人，女性1,929人）のADAMTS13活性の測定を行った[14]。ADAMTS13活性は40%から200%程度まで幅広い分布を示した。男性は女性より活性が低いことが判明した（男性，93±24%，平均値±標準偏差，女性，106±27%，$P<0.0001$）（図1A）。また，30歳台から80歳台までで活性を比較すると，男女ともに加齢により特に60歳以降，活性は低下した（図1B）。80歳台の活性は30歳台の活性の約80%であった。一方，VWF抗原量は加齢により増加するが，今回の集団でもVWF量は加齢により増加し，80歳台のVWF量は30歳台に比べ男性で1.8倍，女性で1.7倍増加していた（図1C）。その結果VWF/ADAMTS13の比は加齢により劇的に増加することが判明した[14]。この比は急性心筋梗塞や肝硬変で上昇するといわれており，高齢者の易血栓性を反映しているものと考えられる。ADAMTS13の活性測定の基質にVWFを用いた場合，検体試料中のVWF濃度が活性に影響することが危惧されていた。しかし，FRETS-VWF73を基質に用いると，ADAMTS13活性は血中VWF濃度に全く影響を受けないことが明らかとなった。また，VWFにはABO型糖鎖が結合しているので，血中VWF濃度はO型で低いことが知られている。私達の測定でも，O型の人のVWF濃度は明らかな低値を示したが，ADAMTS13活性はABO型で影響を受けなかった。

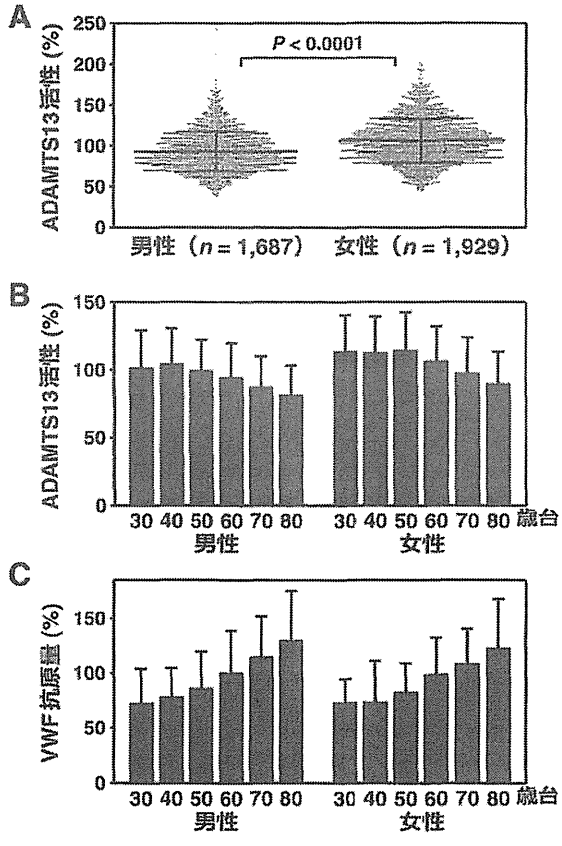

図1 日本人一般住民のADAMTS13活性とVWF抗原量[14]
A. FRETS-VWF73を用いて測定したADAMTS13活性。男性のADAMTS13活性は女性の活性より低い。
B. 年齢別のADAMTS13活性。
C. 性別に分けた年齢別のVWF抗原量。

次に一般住民でのADAMTS13活性値を用いて，先天性ADAMTS13欠損症の頻度の推定を行った[15]。一般住民3,200人（男性1,500人，女性1,700人）から，最も活性の低い32人，次いで活性の低い32人，中央値の活性を示す32人，最も活性の高い32人（各群，男性15人，女性17人）合計128人を選び，ADAMTS13の蛋白質コード領域の全塩基配列の決定を行った。その結果，活性最低値群に7つのまれなミスセンス変異・ノンセンス変異・フレームシフト変異，次低値群に3つのまれなミスセンス変異・フレームシフト変異，活性中央値群と活性高値群にそれぞれ2つのまれなミスセンス変異を同定した。この結果から，32人中には活性に影響を与えないまれなミスセンス変異が2つ存在すると考えられた。これを考慮すると，活性最低値群に5アレル，および活性次低値群に1アレルの機能消失を伴なうと考えられる変異アレルが同定されたこととなる。すなわち，対象とした3,200人中に6人（すなわち533人に1人）のADAMTS13欠損症ヘテロ接合体の存在が推定された。この頻度は家族性高脂血症の頻度によく一致する。これより，TTPの発症に繋がるADAMTS13欠損症ホモ接合体もしくは複合ヘテロ接合体の頻度は110万人に1人と推定され，日本人には約110人の先天性ADAMTS13欠損症の存在が推定された[15]。これまでのところ，日本人には43人の先天性ADAMTS13欠損症患者が報告されている[9]。

ADAMTS13の東アジア人特有のミスセンス変異，P475S変異

私達は先天性ADAMTS13欠損症の遺伝子解析を行なう過程で，東アジア人特有のミスセンス変異，P475S，を同定した[8]。日本人約10人に1人が本変異のヘテロ接合体である。一般住民を対象にした研究から，P475S変異ヘテロ接合体はADAMTS13活性が約17%低下していることが判明した[15]。組換え変異体（MDTCS-P475S）は野生型に比べFRETS-VWF73に対してKm値

が2倍大きくなっていたがKcat値は変化しなかった。組換え変異体はずり応力をかけたVWFを切断した。これらの結果より，本変異保有者はADAMTS13活性を保持しており，本変異が直接TTPのリスクにはならないと考えられた。

ADAMTS13によるVWFの切断メカニズム：ずり応力による基質VWFA2ドメインのアンフォールドとADAMTS13による複数のエクソサイトを介した結合

先に述べたように，ADAMTS13による基質VWFの切断にはVWFの73残基が必要であり，より短い64残基にするともはや切断しない。例えば，トロンビンは3残基から成る合成基質を効率良く切断するし，凝固Xa因子は4残基から成る基質を切断する。ADAMTS13が73残基という長いアミノ酸配列を要求することは，これまでの凝固プロテアーゼの基質認識とは異なったメカニズムによる切断が考えられた。そこで，ADAMTS13の立体構造の解析を行った。ADAMTS13は1,427残基で明らかなドメイン構造からなる（図2A）。MDTCS領域は全長ADAMTS13とほぼ同程度の活性を示す[16]。また，SドメインにはADAMTS13の活性中和自己抗体の結合部位の存在が指摘されていた[16]。そこで，MDTCS領域を培養細胞で発現させ結晶化を試みた。しかし，不溶性のため結晶化には至らなかった。そこでDTCS領域の結晶化とその構造解析を行った[17, 18]。

ADAMTS13-DTCSはD，C_A，Sという3つの球状ドメインがTとC_Bという長いドメインで連結している構造をとっていた[17]（図2B）。結晶構造解析からCドメインはC_AとC_Bから成ることが判明した。Dドメインはディスインテグリン様構造をとらず，C_Aドメインと似たフォールディングをしていた。後天性TTP患者に見られるADAMTS13の活性阻害自己抗体（抗ADAMTS13抗体）のエピトープがSドメインに報告さ

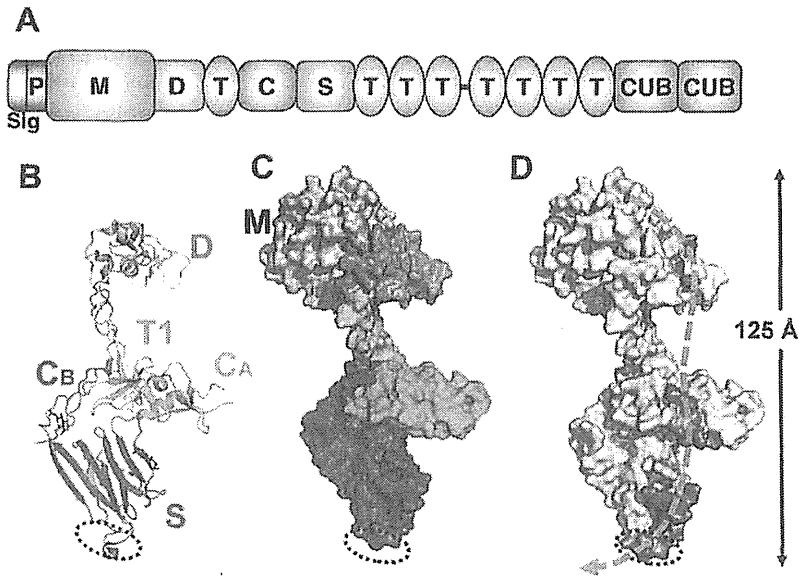

図2 ヒトADAMTS13のドメイン構造と部分立体構造

A. ADAMTS13のドメイン構造。MDTCS領域は全長ADAMTS13とほぼ同等の活性を示す。ADAMTS13は，N末端から，メタロプロテアーゼドメイン（M），ディスインテグリン様ドメイン（D），トロンボスポンジン1 I型リピートドメイン（T），Cys-richドメイン（C），スペーサードメイン（S），7つのTドメイン，2つのCUBドメインから成る。シグナル配列（Sig）とプロ配列（P）は生合成過程で切断される。

B. X線結晶構造解析で決定したADAMTS13のDTCS領域の立体構造[17]。Sドメイン先端の点線で囲んだループ（Arg660，Tyr661，Tyr665を含む）に自己抗体が結合するとTTPを発症する[19]。

C. メタロプロテアーゼ（M）ドメインの構造をモデリングしDTCSに結合させたMDTCSモデル。

D. MDTCS構造中の3つのエクソサイトを赤色および赤茶色で示した。このエクソサイトにVWFの73残基が結合する。基質であるVWFはオレンジ色で示した様にMDTCSに結合すると考えられる。

れ[19]，このエピトープはSドメインの先端に位置することが判明した（図2B）。結晶構造で決定したDTCS構造にMドメインをモデリングにより連結させたMDTCS領域の構造を図2Cに示す[17,20]。この図から，自己抗体の結合部位であるSドメインの先端とMドメインの活性中心は120Å程度離れているにもかかわらず，抗体の結合によりADAMTS13活性が阻害されることが判明した。次いで，MDTCS領域の分子表面に位置するアミノ酸残基や複数のアミノ酸から構成されるループに変異を導入し，FRETS-VWF73基質を用いて変異の影響を調べた。その結果，VWFへの結合にかかわる3つの領域（エクソサイトとよぶ）が存在することが判明した（図2Dの赤および赤茶色で示す部分）。なかでもSドメイン中のエクソサイトは自己抗体結合部位と重複しており，このエクソサイトに抗体が結合すると活性が阻害されることをうまく説明した[17]。

ADAMTS13によるVWFの切断において重要なポイントは，酵素であるADAMTS13は活性型として血中に循環しており，基質であるVWFの切断されるペプチド結合は分子内部に隠れているという点である。立体構造から明らかなように，ADAMTS13の3つのエクソサイトは露出していて基質を結合する準備ができており，メタロプロテアーゼドメインは触媒活性を示す。しかし，切断されるペプチド結合はA2ドメインの内部に埋っており，切断を受けるにはA2ドメインがアンフォールドを起こしてTyr1605-Met1606結合が露出する必要がある。生体内では，血流により生じるずり応力がA2ドメインをアンフォールドし，Tyr1605-Met1606結合を露出させ，ADAMTS13がこの結合を切断すると考えられている。ごく最近，A2ドメインの立体構造が決定された[21]。A2ドメインはジスルフィド結合を持たないのでアンフォールドしやすいと考えられていたが，結晶構造のデータでは，切断部位を含むC末端のペプチドの温度因子が高く，この部分はアンフォールドしやすいことが判明した[21]。また，レーザーピンセットを用いた実験から，単独のA2ドメインは11 pN程度の力でアンフォールドすることも明らかにされた[22]。

ADAMTS13ノックアウトマウスおよびADAMTS13 C末端ドメイン欠損マウスの血栓能の評価を通したADAMTS13の抗血栓能の確立

私達はADAMTS13遺伝子欠損マウスを作製しその表現型を解析した[23]。遺伝子欠損マウスは正常に妊娠出産し，産仔も正常に成長した。欠損ホモ体はメンデルの法則にしたがった数で出産した。欠損マウスの血中には超高分子量VWFマルチマーの蓄積を認めたが，TTP様の微小血管内血小板血栓は観察されなかった[23]。ミシガン大学のグループもADAMTS13ノックアウトマウスを作製したが，彼らのマウスもTTP様の血栓を示さなかった[24]。私達はノックアウトマウスの作製の過程でマウスADAMTS13のcDNAクローニングを行ったところ，系統特異的にトランスポゾンが挿入され，C57BL/6などではC末端に位置する2つのTドメインと2つのCUBドメインが欠損したADAMTS13を持つことを明らかにした[25]。そこで，C末端ドメインを欠損するC57BL/6マウスを，全長ADAMTS13を持つ129/Svマウスに10世代戻し交配することでC末端欠損ADAMTS13をもつ129/Svマウスを作製し，野生型129/Svマウスおよび129/Sv遺伝型背景を持つADAMTS13欠損マウスと血栓能を比較した[26,27]。

図3Aに，高ずり応力（5,000秒$^{-1}$）下の*in vitro*血栓形成能を示す。これはコラーゲンを固相化した平行板型フローチャンバーに蛍光標識した血小板を含む全血を流し，ずり応力下での血小板血栓形成をモニターしたものである。ノックアウトマウス（−/−）は最も血栓量が大きく血栓能が高く，野生型マウス（L/L）は最も血栓量が少ない。このことは，ADAMTS13は抗血栓因子として働き，血小板血栓の形成を抑制することを示している。一方，C末端欠損マウス（S/S）の80秒後の血栓量は野生型より有意に大きな血栓を示した。この差は2,000秒$^{-1}$のずり応力では観察されず，5,000秒$^{-1}$という高ずり応力下ではじめて観察されたので，ADAMTS13のC末端領域は高ずり応力下で抗血栓性を発揮することが明らかになった[26]。

次いで，塩化鉄による血管障害モデルを用いて，血管の閉塞に至るまでの時間を測定することにより3種のマウスの血栓能を評価した（図3B）。野生型マウス（L/L）は障害血管が閉塞されるまでに最も長い時間を必要とし，ノックアウトマウス（−/−）は最も早く閉塞した。C末端欠損マウス（S/S）はその中間であった。野性型マウスが血管閉塞に至るまでに長い時間を必要とすることは，ADAMTS13が抗血栓因子として働き，血管閉塞に抵抗することを示している。私達のこの結果は，平行板型フローチャンバーを用いて以前に示されていた現象，すなわちADAMTS13は高ずり応力がかかる血栓成長部位での血栓の成長を阻止する，という知見を強く支持している[28]。コラーゲンとエピネフリンの混液を静注し，血小板数の減少を調べた実験では，野生型＞C末端欠損型＞ノックアウトの順に，血小板減少の重症度が増大した（図3C）。

TTP様症状を示す動物モデルは有用である。ADAMTS13ノックアウトマウスはTTP様の症状を示さないことを述べた[23]。このマウスにTTP様症状を起こさせるには，高い濃度のVWFを持つCASAマウスとの

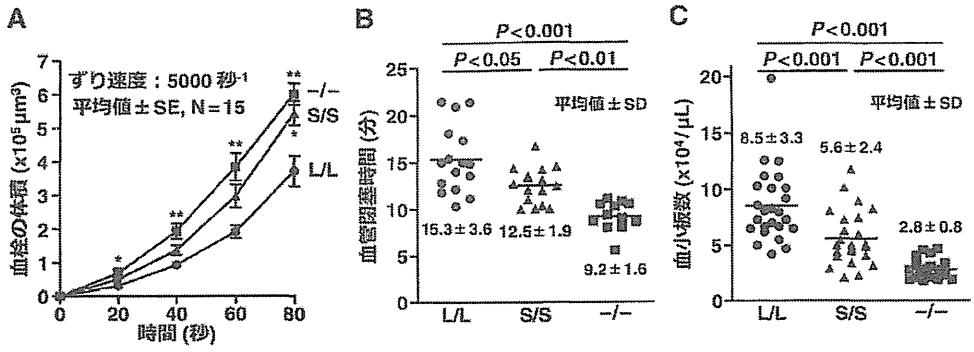

図3　ADAMTS13 ノックアウトマウスと ADAMTS13 C 末端欠損マウスの抗血栓能[26]

A. 平行板型フローチャンバーを用いた固定化コラーゲン上の血小板血栓量。ずり速度：5,000 秒$^{-1}$，−/−：ノックアウトマウス，S/S：C 末端欠損マウス，L/L：野生型マウス。

B. 塩化鉄による腸間膜細動脈障害後の血流の停止までにかかる時間の比較。血流の停止が 30 秒以上になるまでに要する時間を求めた。

C. コラーゲン・エピネフリンの静注による血小板数の減少。

交配[24]，溶血性尿毒症症候群の原因となるシガ毒素の静注[24, 29]，ADAMTS13 抗体の静注，といった方法がある。また，ヒヒに抗ヒト ADAMTS13 抗体を静注するとTTP 様の症状を示す[30]。

ADAMTS13 が VWF マルチマーを切断するメカニズム

VWF マルチマーが ADAMTS13 により切断を受けるメカニズムは次のように考えられる。血漿中の ADAMTS13 の約 5%は VWF と結合した状態で循環している[31, 32]。この結合は ADAMTS13 の C 末端領域のドメインと VWF の C 末端領域のドメインの間で行われる（図 4 ①）。前述したように，C 末端ドメイン欠損 ADAMTS13をもつマウス（C57BL/6 マウスなど）は全長ADAMTS13をもつマウスに比べ血管閉塞に要する時間の短縮などが見られ，抗血栓能の低下が観察された。このことから，血管内での血小板血栓形成において，ADAMTS13の C 末端ドメインは一定の働きをしていることが理解された。図 4 ②に示すように，VWF の A2 ドメイン内の ADAMTS13 切断部位（Tyr1605-Met1606 結合）は分子内部に埋れている。A2 ドメインは血管内のずり応力によりアンフォールドし，ADAMTS13 が結合する A2 ドメインの VWF73 領域が露出し（図 4 ③），ADAMTS13 内の 3 つのエクソサイトが VWF73 領域に結合し（図 4 ④），メタロプロテアーゼ（M）ドメインの触媒基により Tyr1605-Met1606 結合が切断される（図 4 ⑤）。このように，ADAMTS13 は N 末端の M ドメインから C 末端の VWF 結合ドメインまで，全領域を使って基質 VWF を認識し 1 ヶ所のペプチド結合を正確に切断する。VWF の血中濃度は約 10 μg/m*l* であり，血漿総タンパク質は約 80 mg/m*l* である。このように，8,000 倍も少ないタンパク質を特異的に切断するために，血中濃度 0.5〜1 μg/m*l* である ADAMTS13[33]は全領域を用いて VWF を認識するよう進化を遂げたものと考えられる。

ADAMTS プロテアーゼは 19 種のファミリータンパク質から成り，全ての ADAMTS プロテアーゼは MDTCS 領域を含む[34]。このファミリーのプロテアーゼはここで述べたように，複数のエクソサイトを介して特異的に基質を認識していると考えられる[17, 18]。ADAMTS13 が VWF 切断酵素としてクローニングされて以来，多くの ADAMTS ファミリータンパク質が疾患に関連すると報告された[34, 35]。こういった疾患発症の解明に DTCS 領域の立体構造の解析が大きく寄与している[35]。

VWF の切断にはずり応力による A2 ドメインのアンフォールドが重要であることを述べた。では，生体内ではどういった場面で VWF にずり応力がかかるのだろうか。VWF はモノマーがジスルフィド結合で架橋されたマルチマーとして血中に分泌される。VWF マルチマーは静止状態ではゆるいコイル状の鳥の巣のような形をしている[36, 37]。生体内の正常血管内で見られる最大のずり応力は，100 dyn/cm^2（ずり速度で 5,000 秒$^{-1}$）といわれる。実験によると，モノマーが 200 個程度繋がった VWF マルチマーの中央にあるモノマーには，10 pN の張力がかかると推定された[22]。単独の A2 ドメインは約 11 pN の張力でアンフォールドし ADAMTS13 により切断を受けると考えられる[22]。血漿中の VWF は最大で〜200 モノマーが繋がっている[36, 37]。これらの結果は血漿中の最大の VWF マルチマーは 200 モノマーからなることをうまく説明している。しかし，A2 ドメインは他

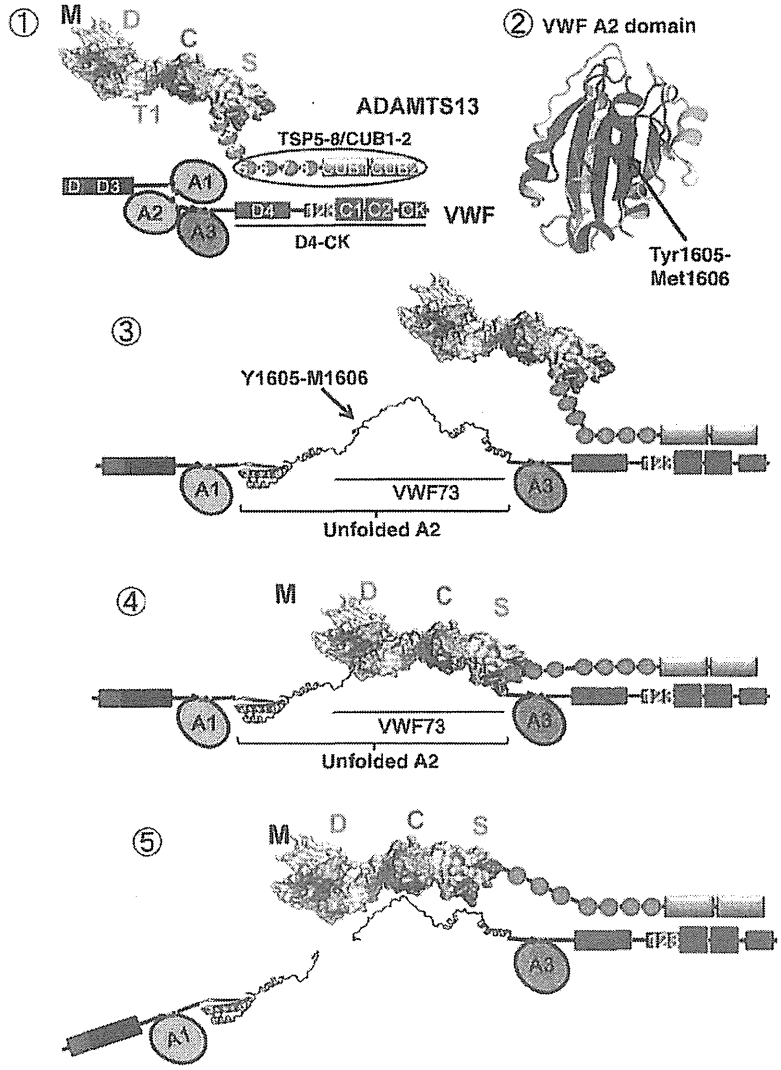

図4 ADAMTS13によるずり応力依存性のVWF切断

② VWF A2ドメインの立体構造[21]。ADAMTS13切断部位であるTyr1605-Met1606結合は分子内に埋れている。A2ドメインはジスルフィド結合を持たない。

①，③～⑤ 約5%のADAMTS13は血漿中でVWFとC末端領域を介して複合体を形成している[31,32]。VWF A2ドメインはずり応力によりアンフォールドし，ADAMTS13結合部位であるVWF73領域が露出する。ここにADAMTS13のD，C，Sドメインにあるエクソサイトが結合し，Mドメインが Y1605-M1606結合を切断する[17]。このように，酵素であるADAMTS13は活性型として血中を循環しており，基質であるVWFがアンフォールドするとA2ドメイン内の特定の残基を切断するという，めずらしい基質切断のメカニズムが明らかとなった。

のドメインで安定化され，アンフォールドに21 pNを要するという研究もあり，より慎重な解釈が求められる[38]。

TTPは微小血管内に閉塞性の血小板血栓を形成するが大血管には血栓は観察されない。微小血管では大血管に比べ大きなずり応力がかかる。高ずり応力がかかったVWFは伸展構造をとり，血小板GPIbαや内皮下層のコラーゲンに結合する部位が露出し血栓能が亢進する。血

小板[39]，内皮下層のコラーゲン[40]，血管内皮細胞[41,42]に結合したVWFは張力をより受けやすく，こういったものに係留されたVWFのA2ドメインはアンフォールドし，ADAMTS13により切断されやすい。通常はADAMTS13での切断により，過度な血小板血栓の形成が抑制されている。しかし，ADAMTS13の重度の欠損症では，血小板やコラーゲン，血管内皮細胞に結合し伸展したVWFでも切断されず，さらに血小板の結合が進むこととなり，閉塞性の血小板血栓へと成長すると考えられる。

おわりに

ADAMTS13を中心に，TTP発症のメカニズムを解説した。2001年にADAMTS13がクローニングされて以来，TTPに関して多くの研究がなされ，TTPの発症メカニズムの理解が大きく進んだ。本稿ではTTPの治療に関して述べなかった。治療に関しては他書を参照されたい[1,43～45]。

著者のCOI（conflicts of interest）開示：本論文発表内容に関連して特に申告なし

文　献

1) Sadler JE. Von Willebrand factor, ADAMTS13, and thrombotic thrombocytopenic purpura. Blood. 2008; **112**: 11-18.
2) 副島見事，小亀浩市，松本雅則. ADAMTS13物語. 日血栓止血会誌. 2009; **20**: 377-397.
3) 松本雅則，藤村吉博. ADAMTS13とTTP最近の進歩. Annu Rev 血液. 2009; **2009**: 209-216.
4) Tsai HM. Pathophysiology of thrombotic thrombocytopenic purpura. Int J Hematol. 2010; **91**: 1-19.
5) Soejima K, Mimura N, Hirashima M, et al. A novel human metalloprotease synthesized in the liver and secreted into the blood: possibly, the von Willebrand factor-cleaving protease? J Biochem. 2001; **130**: 475-480.
6) Levy GG, Nichols WC, Lian EC, et al. Mutations in a member of the ADAMTS gene family cause thrombotic thrombocytopenic purpura. Nature. 2001; **413**: 488-494.
7) Zheng X, Chung D, Takayama TK, Majerus EM, Sadler JE, Fujikawa K. Structure of von Willebrand factor-cleaving protease (ADAMTS13), a metalloprotease involved in thrombotic thrombocytopenic purpura. J Biol Chem. 2001; **276**: 41059-41063.
8) Kokame K, Matsumoto M, Soejima K, et al. Mutations and common polymorphisms in ADAMTS13 gene responsible for von Willebrand factor-cleaving protease activity. Proc Natl Acad Sci U S A. 2002; **99**: 11902-11907.
9) Fujimura Y, Matsumoto M, Isonishi A, et al. Natural history of Upshaw-Schulman syndrome based on ADAMTS13 gene analysis in Japan. J Thromb Haemost. 2011; **9 Suppl 1**: 283-301.
10) Fujimura Y, Matsumoto M, Kokame K, et al. Pregnancy-induced thrombocytopenia and TTP, and the risk of fetal death, in Upshaw-Schulman syndrome: a series of 15 pregnancies in 9 genotyped patients. Br J Haematol. 2009; **144**: 742-754.
11) Bennett CL, Weinberg PD, Rozenberg-Ben-Dror K, Yarnold PR, Kwaan HC, Green D. Thrombotic thrombocytopenic purpura associated with ticlopidine. A review of 60 cases. Ann Intern Med. 1998; **128**: 541-544.
12) Kokame K, Matsumoto M, Fujimura Y, Miyata T. VWF73, a region from D1596 to R1668 of von Willebrand factor, provides a minimal substrate for ADAMTS-13. Blood. 2004; **103**: 607-612.
13) Kokame K, Nobe Y, Kokubo Y, Okayama A, Miyata T. FRETS-VWF73, a first fluorogenic substrate for ADAMTS13 assay. Br J Haematol. 2005; **129**: 93-100.
14) Kokame K, Sakata T, Kokubo Y, Miyata T. von Willebrand factor-to-ADAMTS13 ratio increases with age in a Japanese population. J Thromb Haemost. 2011; **9**: 1426-1428.
15) Kokame K, Kokubo Y, Miyata T. Polymorphisms and mutations of ADAMTS13 in the Japanese population and estimation of the number of patients with Upshaw-Schulman syndrome. J Thromb Haemost. 2011; **9**: 1654-1656.
16) Soejima K, Matsumoto M, Kokame K, et al. ADAMTS-13 cysteine-rich/spacer domains are functionally essential for von Willebrand factor cleavage. Blood. 2003; **102**: 3232-3237.
17) Akiyama M, Takeda S, Kokame K, Takagi J, Miyata T. Crystal structures of the noncatalytic domains of ADAMTS13 reveal multiple discontinuous exosites for von Willebrand factor. Proc Natl Acad Sci U S A. 2009; **106**: 19274-19279.
18) 秋山正志，武田壮一，小亀浩市，高木淳一，宮田敏行. VWF切断酵素ADAMTS13のエキソサイト認識機構. 生化学. 2010; **82**: 950-956.
19) Pos W, Crawley JT, Fijnheer R, Voorberg J, Lane DA, Luken BM. An autoantibody epitope comprising residues R660, Y661, and Y665 in the ADAMTS13 spacer domain identifies a binding site for the A2 domain of VWF. Blood. 2010; **115**: 1640-1649.
20) Takeda S, Takeya H, Iwanaga S. Snake venom metalloproteinases: Structure, function and relevance to the mammalian ADAM/ADAMTS family proteins. Biochim Biophys Acta. 2012; **1824**: 164-176.
21) Zhang Q, Zhou YF, Zhang CZ, Zhang X, Lu C, Springer TA. Structural specializations of A2, a force-sensing domain in the ultralarge vascular protein von Willebrand factor. Proc Natl Acad Sci U S A. 2009; **106**: 9226-9231.
22) Zhang X, Halvorsen K, Zhang CZ, Wong WP, Springer TA. Mechanoenzymatic cleavage of the ultralarge vascular protein von Willebrand factor. Science. 2009; **324**: 1330-1334.
23) Banno F, Kokame K, Okuda T, et al. Complete deficiency in

ADAMTS13 is prothrombotic, but it alone is not sufficient to cause thrombotic thrombocytopenic purpura. Blood. 2006; **107**: 3161-3166.

24) Motto DG, Chauhan AK, Zhu G, et al. Shigatoxin triggers thrombotic thrombocytopenic purpura in genetically susceptible ADAMTS13-deficient mice. J Clin Invest. 2005; **115**: 2752-2761.

25) Banno F, Kaminaka K, Soejima K, Kokame K, Miyata T. Identification of strain-specific variants of mouse Adamts13 gene encoding von Willebrand factor-cleaving protease. J Biol Chem. 2004; **279**: 30896-30903.

26) Banno F, Chauhan AK, Kokame K, et al. The distal carboxyl-terminal domains of ADAMTS13 are required for regulation of *in vivo* thrombus formation. Blood. 2009; **113**: 5323-5329.

27) Banno F, Chauhan AK, Miyata T. The function of ADAMTS13 in thrombogenesis *in vivo*: insights from mutant mice. Int J Hematol. 2010; **91**: 30-35.

28) Shida Y, Nishio K, Sugimoto M, et al. Functional imaging of shear-dependent activity of ADAMTS13 in regulating mural thrombus growth under whole blood flow conditions. Blood. 2008; **111**: 1295-1298.

29) Huang J, Motto DG, Bundle DR, Sadler JE. Shiga toxin B subunits induce VWF secretion by human endothelial cells and thrombotic microangiopathy in ADAMTS13-deficient mice. Blood. 2010; **116**: 3653-3659.

30) Feys HB, Roodt J, Vandeputte N, et al. Thrombotic thrombocytopenic purpura directly linked with ADAMTS13 inhibition in the baboon (Papio ursinus). Blood. 2010; **116**: 2005-2010.

31) Feys HB, Anderson PJ, Vanhoorelbeke K, Majerus EM, Sadler JE. Multi-step binding of ADAMTS-13 to von Willebrand factor. J Thromb Haemost. 2009; **7**: 2088-2095.

32) Zanardelli S, Chion AC, Groot E, et al. A novel binding site for ADAMTS13 constitutively exposed on the surface of globular VWF. Blood. 2009; **114**: 2819-2828.

33) Soejima K, Nakamura H, Hirashima M, Morikawa W, Nozaki C, Nakagaki T. Analysis on the molecular species and concentration of circulating ADAMTS13 in Blood. J Biochem. 2006; **139**: 147-154.

34) Apte SS. A disintegrin-like and metalloprotease (reprolysin-type) with thrombospondin type 1 motif (ADAMTS) superfamily: functions and mechanisms. J Biol Chem. 2009; **284**: 31493-31497.

35) Kuchtey J, Olson LM, Rinkoski T, et al. Mapping of the disease locus and identification of ADAMTS10 as a candidate gene in a canine model of primary open angle glaucoma. PLoS Genet. 2011; **7**: e1001306.

36) Fowler WE, Fretto LJ, Hamilton KK, Erickson HP, McKee PA. Substructure of human von Willebrand factor. J Clin Invest. 1985; **76**: 1491-1500.

37) Schneider SW, Nuschele S, Wixforth A, et al. Shear-induced unfolding triggers adhesion of von Willebrand factor fibers. Proc Natl Acad Sci U S A. 2007; **104**: 7899-7903.

38) Ying J, Ling Y, Westfield LA, Sadler JE, Shao JY. Unfolding the A2 domain of von Willebrand factor with the optical trap. Biophys J. 2010; **98**: 1685-1693.

39) Shim K, Anderson PJ, Tuley EA, Wiswall E, Sadler JE. Platelet-VWF complexes are preferred substrates of ADAMTS13 under fluid shear stress. Blood. 2008; **111**: 651-657.

40) Bonnefoy A, Romijn RA, Vandervoort PA, VAN Rompaey I, Vermylen J, Hoylaerts MF. von Willebrand factor A1 domain can adequately substitute for A3 domain in recruitment of flowing platelets to collagen. J Thromb Haemost. 2006; **4**: 2151-2161.

41) Padilla A, Moake JL, Bernardo A, et al. P-selectin anchors newly released ultralarge von Willebrand factor multimers to the endothelial cell surface. Blood. 2004; **103**: 2150-2156.

42) Huang J, Roth R, Heuser JE, Sadler JE. Integrin alpha (v) beta (3) on human endothelial cells binds von Willebrand factor strings under fluid shear stress. Blood. 2009; **113**: 1589-1597.

43) George JN. Clinical practice. Thrombotic thrombocytopenic purpura. N Engl J Med. 2006; **354**: 1927-1935.

44) Zakarija A, Kwaan HC, Moake JL, et al. Ticlopidine- and clopidogrel-associated thrombotic thrombocytopenic purpura (TTP): review of clinical, laboratory, epidemiological, and pharmacovigilance findings (1989～2008). Kidney Int Suppl. 2009: S20-24.

45) Kiss JE. Thrombotic thrombocytopenic purpura: recognition and management. Int J Hematol. 2010; **91**: 36-45.

Thrombosis Research 129 (2012) e200–e208

Contents lists available at SciVerse ScienceDirect

Thrombosis Research

journal homepage: www.elsevier.com/locate/thromres

A novel *ENG* mutation causing impaired co-translational processing of endoglin associated with hereditary hemorrhagic telangiectasia

Atsuo Suzuki [a], Daisuke Nakashima [a], Yuhri Miyawaki [a], Junko Fujita [a], Asuka Maki [a], Yuta Fujimori [a], Akira Takagi [a,b], Takashi Murate [a,b], Masaaki Teranishi [c], Tadashi Matsushita [d], Hidehiko Saito [e], Tetsuhito Kojima [a,b,*]

[a] *Department of Pathophysiological Laboratory Sciences, Nagoya University Graduate School of Medicine, 1-1-20 Daiko-Minami, Higashi-Ku, Nagoya 461–8673, Japan*
[b] *Department of Medical Technology, Nagoya University School of Health Sciences, 1-1-20 Daiko-Minami, Higashi-Ku, Nagoya 461–8673, Japan*
[c] *Department of Otorhinolaryngology, Nagoya University Graduate School of Medicine, 65 Tsurumai-Cho, Showa-Ku, Nagoya 466–8550, Japan*
[d] *Division of Transfusion Medicine, Nagoya University Hospital, 65 Tsurumai-Cho, Showa-Ku, Nagoya 466–8550, Japan*
[e] *Nagoya Medical Center, 4-1-1 San-no-maru, Naka-Ku, Nagoya 460–0001, Japan*

ARTICLE INFO

Article history:
Received 27 September 2011
Received in revised form 21 November 2011
Accepted 22 December 2011
Available online 3 March 2012

Keywords:
hereditary hemorrhagic telangiectasia
endoglin
signal peptide
co-translational processing
endoplasmic reticulum

ABSTRACT

Hereditary hemorrhagic telangiectasia (HHT) is an inherited autosomal dominant vascular dysplasia caused by mutations in mainly the endoglin gene (*ENG*) or activin-like kinase receptor 1 (ALK1) gene (*ACVRL1*). We investigated the molecular basis of HHT in a Japanese patient, and identified a novel missense mutation in *ENG* (c.38 T>A, p.Leu13Gln) located in the signal peptide's hydrophobic core, but not in *ACVRL1*. In experiments in COS-1 cells, the Leu13Gln (L13Q) mutant endoglin appeared to be expressed as a precursor form, probably due to impaired protein processing. Flow cytometry analyses of the COS-1 cells transiently expressing recombinant endoglins revealed that the wild-type endoglin was detected on the cell surface, but the L13Q mutant was not. We also analyzed expression patterns of the recombinant endoglins by immunofluorescent staining, and found that the wild-type co-localized with the endoplasmic reticulum (ER), but the L13Q mutant did not. These results implied that the L13Q mutant endoglin fails to insert into the ER, probably due to destruction of the hydrophobic core structure in the signal peptide to be recognized by signal recognition particles. Thus, the Leu13 in the signal peptide of endoglin might be essential for correct protein processing through the ER and cell-surface expression. Taken together, the novel c.38 T>A mutation in *ENG* would impair co-translational processing of the endoglin, and could be responsible for HHT in this patient.

Hereditary hemorrhagic telangiectasia (HHT), also known as Osler-Rendu-Weber syndrome, is an inherited autosomal dominant vascular dysplasia with a frequency of 1 in 10,000, and exhibits age-related penetrance with variable expressivity [1-3]. The most common clinical manifestations involve the development of vascular abnormalities seen as telangiectases on skin and lesions in nasal mucosa that readily bleed. Further clinical manifestations are pulmonary, cerebral, hepatic and, in rare cases, spinal cord arteriovenous malformations. These may cause serious complications such as stroke, brain abscess, hemorrhage, or venous thromboembolism [4-6].

HHT type 1 (HHT1) is caused by a mutation in the gene encoding endoglin (*ENG*) located on the long arm of chromosome 9 (9q34) [7-9]. HHT type 2 (HHT2) is caused by a mutation in the activin-like kinase receptor 1 (ALK1) gene (*ACVRL1*) located on the long arm of chromosome 12 (12q13) [10-12]. Many mutations have been identified in *ENG* and *ACVRL1* genes and support the haploinsufficiency model for HHT, that is that the remaining wild-type allele is unable to contribute sufficient protein for normal function [13]. Endoglin is a homodimeric integral membrane glycoprotein that interacts with signaling receptor complexes for several members of the transforming growth factor-β (TGF-β) superfamily, and composed of disulfide-linked 90-kDa subunits [14-16]. It is expressed primarily in the vascular endothelial cells of capillaries, arterioles, and venules, as well as in activated monocytes, syncytiotrophoblasts, and some leukemic cells. Two alternatively spliced variants, long- and short-form endoglins, are encoded by *ENG*. It is suggested that short-form endoglin is induced during endothelial senescence and plays opposite roles with respect to the predominant long-form endoglin, contributing to age-dependent vascular pathology [13].

Abbreviations: ALK1, activin receptor-like kinase-1; HHT, hereditary hemorrhagic telangiectasia; HHT1, HHT type 1; TGF-β, transforming growth factor-βSRP., signal recognition particle; RFLP, restriction fragment-length polymorphism; DMEM, Dulbecco's modified Eagle's medium; FBS, fetal bovine serum; SDS, sodium dodecyl sulfate; SDS-PAGE, SDS-polyacrylamide gel electrophoresis; ER, endoplasmic reticulum; RT, room temperature; PBS, phosphate-buffered saline; DMSO, dimethyl sulfoxide; DAPI, 4'6-diamidino-2-phenylindole-2HCl.

* Corresponding author at: Department of Medical Technology, Nagoya University School of Health Sciences, 1-1-20, Daiko-Minami, Higashi-ku, Nagoya 461–8673, Japan. Tel./fax: +81 52 719 3153.
E-mail address: kojima@met.nagoya-u.ac.jp (T. Kojima).

0049-3848/$ – see front matter © 2011 Elsevier Ltd. All rights reserved.
doi:10.1016/j.thromres.2011.12.030

ALK1 is also expressed on endothelial cells, and is a type I receptor of the TGF-β superfamily [17].

TGF-β family cytokines are multifunctional proteins that regulate proliferation, differentiation, migration, adhesion and apoptosis of various cell types, and mediate their cellular effects through a heteromeric complexes of type I and type II transmembrane serine-threonine kinase receptors [5]. Ligand binding induces association of the type I and type II receptors, leading to a unidirectional phosphorylation event in which the type II receptor phosphorylates the type I receptor, thereby activating its kinase domain. The activated type I receptor phosphorylates receptor regulated Smads (R-Smads) and these activated R-Smads bind subsequently to the common mediator (Co-Smad), Smad4. The R-Smad/Co-Smad complexes accumulate in the nucleus where it regulates transcription by interacting with many specific DNA-binding proteins. Although the core of the TGF-β receptor complex is formed by the association of type I and type II receptors, it may also contain auxiliary receptors such as endoglin. In endothelial cells (ECs), the TGF-β type II receptor and two distinct TGF-β type I receptors, the EC-restricted ALK1 and the broadly expressed ALK5, are expressed [18,19]. Endoglin is necessary for efficient TGF-β/ALK1 signaling and indirectly inhibits TGF-β/ALK5 signaling, thereby promoting the activation state of EC during angiogenesis [20].

To date, 282 different mutations have been reported in the *ENG* gene and 246 distinct mutations in the *ACVRL1* gene (human gene mutation database: HGMD, http://www.hgmd.cf.ac.uk/ac/all.php). Some missense mutations in the signal peptide region of endoglin have been reported, but their molecular basis has yet to be investigated in detail. In this study, we analyzed the *ENG* gene in a Japanese patient with HHT, and found a novel missense mutation in the signal peptide region of endoglin. We further investigated the molecular basis of HHT in the patient through expression analyses of the mutant endoglin in COS-1 cells.

1. Materials and Methods

1.1. Sample preparation

Ethical approval for this study was obtained from the Ethics Committee of the Nagoya University School of Medicine. Citrated blood samples were obtained from the patient and his sister with informed consent. Genomic DNA was isolated from the peripheral leukocytes by phenol extraction.

1.2. Polymerase Chain Reaction (PCR) and DNA sequencing

The protein-coding exons and exon-intron boundaries of *ENG* and *ACVRL1* were amplified by the polymerase chain reaction (PCR) using gene-specific primers (Suppl. Table 1). The PCR products were electrophoresed on agarose gels, and purified with a QIAEX II Gel Extraction Kit (QIAGEN, GmbH, Germany). We performed direct sequencing of the purified PCR products with a Big Dye Terminator Cycle Sequencing Kit (Applied Biosystems, Foster City, CA) and ABI Prism 310 Genetic Analyzer (Applied Biosystems).

1.3. PCR-Restriction Fragment Length Polymorphism (RFLP) analysis

PCR-mediated restriction fragment length polymorphism (PCR-RFLP) was performed to detect the missense mutation (c.38 T>A) identified in the *ENG* gene of the patient. Briefly, we amplified a part of the *ENG* gene containing the c.38 T>A mutation by PCR using an exon 1 sense primer and a partially mismatched antisense primer (5'-GACACCTACTTGTGGGGCTGAGGGTGC-3': the mutated nucleotide is underlined), which was designed to destroy the *Pst*I site near the mutation. The PCR products were digested with *Pst*I and analyzed by electrophoresis on 3% NuSieve 3:1 agarose (LONZA, Walkersville, MD).

1.4. Cell culture and reagents

African green monkey kidney COS-1 cells were purchased from the American Type Culture Collection (ATCC, Manassas, VA). The EAhy926 cells, which are human umbilical vein endothelial cell (HUVEC)-like cells, were generously donated by Dr. Cora-Jean S. Edgell (University of North Carolina, Chapel Hill, NC). The cells were cultured in Dulbecco's Modified Eagle's Medium (DMEM) (Wako, Tokyo, Japan) supplemented with 10% fetal bovine serum (FBS; CCB from Nichirei Biosciences, Tokyo, Japan) and 100× antibiotic-antimycotic mixed stock solution (Nacalai Tesque, Kyoto, Japan). Tunicamycin was purchased from Sigma-Aldrich (St Louis, MO), and dissolved in Hybri-Max® DMSO (Sigma-Aldrich).

1.5. Construction of the endoglin expression vector and transient transfection

Full-length human endoglin cDNAs, encoding the 658-amino acid long form (L-ENG) and 625-amino acid short form (S-ENG), were prepared by reverse transcription (RT)-PCR from normal peripheral mononuclear cell mRNAs. These cDNAs were inserted into the pCI Mammalian Expression Vector (Promega, Madison, WI) between *Eco*RI and *Sal*I sites (pL-ENG^{WT} and pS-ENG^{WT}).

To introduce a c.38 T>A transversion, we used a Quik Change Lightning Site-Directed Mutagenesis kit (Stratagene, La Jolla, CA) according to the manufacturer's instructions, with the following primers; 5'-GTTGCCCTGCAGCTGGCCAGCTGCAGCC-3' (sense: the mutated nucleotide is underlined), 5'-GGCTGCAGCTGGCCAGCTG CAGGGCAAC-3' (antisense), and prepared L13Q mutant endoglin expression vectors (pL-ENG^{L13Q} and pS-ENG^{L13Q}).

For transient transfection, COS-1 cells were seeded at a concentration of 5×10^5 cells in 60 mm dishes or 2×10^5 cells in 35 mm dishes. After 18 hr, the respective endoglin expression vector or a mock vector (pCI) (0.5 μg or 5 μg in 60 mm dish, or 1 μg in 35 mm dish) was transfected using Lipofectoamine2000 reagent (Invitrogen, Carlsbad, CA) according to the manufacturer's directions. Following experiments were performed at 48 hr after transfection.

1.6. Western Blot analysis

The transfected cells were lysed in SDS sample buffer with or without β-mercaptoethanol (β-ME), boiled, and subjected to 10% SDS-PAGE followed by Western blotting. The Western blot was performed as described previously [21] with minor modifications. Primary antibody against endoglin (H-300; Santa Cruz Biotechnology, Santa Cruz, CA), β-actin (Cytoskeleton, Denver, CO), Smad3 or phospho-Smad3 (Cell Signaling Technology, Danvers, MA) was probed in a dilution of 1:1000, and after being washed, horseradish peroxidase-conjugated secondary antibody (Cell Signaling Technology) was probed. Signals were visualized with a chemiluminescent HRP substrate on Immobilon™-Western (Millipore Corp., Billerica, MA). The intensities of the bands were quantified by ATTO CS analyzer (ATTO, Tokyo, Japan) and represented as relative values of endoglin against β-actin, respectively.

1.7. Flow cytometry analysis and Cell-surface biotinylation-immunoprecipitation (IP) analysis

COS-1 cells were transiently transfected with 1 μg of pL-ENG^{WT} or pL-ENG^{L13Q} in 35 mm dish, and harvested using 1 mM EDTA in PBS after 48 hr. The cells were washed with PBS, and resuspended in flow cytometry buffer (1% FBS, 0.1% NaN_3 in PBS). The cells in flow cytometry buffer were divided into aliquots, and treated with blocking buffer (1% BSA in flow cytometry buffer) for 15 min at room temperature (RT). After centrifugation, the cells were incubated with anti-endoglin antibody (H-300; a rabbit polyclonal antibody raised against amino acids 27–326 of human endoglin, Santa Cruz Biotechnology) or isotype-matched rabbit IgG (10 μg/mL) in blocking buffer for 15 min at RT. Anti-rabbit IgG-Alexa488 antibody (Invitrogen) was

incubated for 15 min at RT after 2 washes with flow cytometry buffer, and the cells were analyzed in FACS Calibur (BD biosciences, Franklin Lakes, NJ).

We also biotinylated the cell surface molecules of the COS-1 cells transfected with pL-ENG^{WT} or pL-ENG^{L13Q} by incubation for 1 hr at RT in PBS containing 0.5 mg/ml *N*-hydroxysuccinimidobiotin (EZ-Link® NHS-Biotin Reagents; PIERCE, Rockford, IL). Recombinant endoglins in the soluble fractions of harvested cell lysates were immunoprecipitated by anti-endoglin antibody (H-300; Santa Cruz Biotechnology) and subjected to 10% SDS-PAGE. Biotinylated proteins were then detected as chemiluminescent signals using streptavidin-HRP conjugates (Amersham Biosciences) in a Western blot analysis as described above.

1.8. Immunofluorescence staining

COS-1 cells were transiently transfected with either pL-ENG^{WT} or pL-ENG^{L13Q}. After 24 hr, the cells were replated and grown on 18x18mm cover glasses that were coated with collagen I (Nippi, Tokyo, Japan). Forty-eight hours after transfection, the cells were washed with PBS, fixed in cold methanol, and permeabilized with cold acetone. After a blocking procedure in PBS containing 1% BSA (1%BSA-PBS) for 30 min, the cells were incubated with 1:100 diluted rabbit anti-endoglin antibody (H-300; Santa Cruz Biotechnology), mouse anti-β-actin antibody, mouse anti-alpha 1 sodium potassium ATPase antibody (Abcam, Cambridge, UK) or anti-protein disulfide isomerase (PDI) antibody (Stressgen Bioreagents, Ann Arbor, MI) in 1%BSA-PBS for 1 hr at RT. After 3 washes with PBS, the cells were incubated with 1:100 diluted anti-rabbit IgG-Alexa488 antibody (Invitrogen) or anti-mouse IgG-Alexa555 antibody (Invitrogen) in 1%BSA-PBS for 1 hr at RT. After another 3 washes with PBS, the cells were enclosed by VECTASHIELD with DAPI (Vector Laboratories, Inc. Burlingame, CA), and inspected by fluorescence microscopy (PROVIS AX80, OLYMPUS, Tokyo, Japan).

1.9. Glycosylation inhibition experiments

COS-1 cells were transfected with pL-ENG^{WT} or pL-ENG^{L13Q} in 35 mm dish as described above. After 24 hr, they were treated with 1 to 10 μg/mL tunicamycin for 24 hr, lysed, and subjected to Western blotting as described above.

2. Results

2.1. Case report

The patient was a 61-year-old man, who had mucocutaneous telangiectasia on his fingers and tongue, pulmonary arteriovenous malformations, and recurrent episodes of frequent nasal bleeding. His father, two of five sisters, and his son also suffered from recurrent nasal bleeding. As showing epistaxis, telangiectases, lung arteriovenous malformations and familiar bleeding history, he was diagnosed with HHT according to Curaçao criteria [5] and treated through ultrasonic coagulation of the nasal mucosa.

2.2. Sequencing of ENG and ACVRL1, and PCR-RFLP

Direct sequencing of the proband's *ENG* and *ACVRL1* genes revealed a novel missense mutation in exon 1 of *ENG* as a heterozygous form, but no mutation in *ACVRL1*. The mutation was a T-to-A transversion at nucleotide 38 in the coding sequence of *ENG* (c.38 T>A), replacing leucine 13 (CTG) with a glutamine (CAG) (p.Leu13Gln) in the hydrophobic core region of the endoglin signal peptide (Fig. 1). We detected the same mutation in his sister (data not shown). We further performed a mismatch PCR-mediated *PstI*-RFLP analysis to detect the c.38 T>A mutation, as described in Materials and Methods. The sample from the patient showed two bands, which were cleaved 225 bp (mutant allele) and uncleaved 263 bp (normal allele) bands, while that from a healthy individual showed only an uncleaved 263 bp band (Suppl. Fig. 1), confirming that the proband was heterozygous for this mutation. We also analyzed 100 samples of healthy individuals, and observed that all samples showed a normal pattern with a single band of 263 bp (data not shown).

2.3. Western blot analysis of recombinant endoglins expressed in COS-1 cells

To examine the effects of the L13Q missense mutation on the structure and function of endoglins, we expressed the mutant and wild-type endoglins (long-form; L-ENG, short-form; S-ENG) in COS-1 cells, and compared them by Western blotting. Under reducing conditions, the recombinant wild-type long-form endoglin (L-ENG) showed 3 bands, whereas the L13Q mutant showed only a smaller band (Fig. 2A). We also compared the long-form (L-ENG) and short-form (S-ENG), and found that they showed a similar 3-band pattern with different sizes depending on the number of amino acids. The endogenous endoglin from EAhy926 cells possessed a single band equal in size to a larger band of recombinant L-ENG. Therefore, we further analyzed long forms of the recombinant endoglins expressed in COS-1 cells. Under non-reducing conditions, Western blotting revealed that the wild-type L-ENG showed two bands representing a protein dimer, with the larger bands getting more intense in a time-dependent manner, which were similar in size to the endogenous endoglin from EAhy926 cells (Fig. 2B). However, the L13Q mutant mostly retained a smaller 60 kDa band at 72 hr after transfection, indicating that the L13Q mutation impaired the dimerization of recombinant endoglin. The intensity of L13Q band was so low in the non-reducing gel but not in the reducing gel, although the reason for this reproducible phenomenon is unclear.

2.4. Impaired cell surface expression of the L13Q mutant in COS-1 cells

We next investigated whether recombinant endoglins were expressed on the surface of COS-1 cells, transfected with the respective expression vectors, by flow cytometry using anti-endoglin antibody. As shown in Fig. 3A, over 25% of the cells transfected with pL-ENG^{WT} were positive for endoglin expression on the cell surface, whereas less than 3% of the cells transfected with pL-ENG^{L13Q} were positive. We verified the transfection efficiency in COS-1 cells with a GFP-expression vector, and found that about 20 to 30% of the cells were positive (data not shown). Considering the transfection efficiency, most of the cells expressing the wild-type recombinant endoglin were positive for its cell surface expression, but most of the cells expressing L13Q mutant were not. These results suggested that the L13Q mutation might severely impair endoglin expression on the cell surface.

We tested the cell-surface expression of recombinant endoglins by immunofluorescence analysis (Fig. 3B). To determine the localization of recombinant endoglins on the cell membrane, we performed co-staining of recombinant endoglins (green) with a membrane marker Na-K-ATPase (red) using the respective specific antibodies. As a result, wild-type endoglin was detected all over the cell bodies and co-localized with Na-K-ATPase on a part of the cell surface (yellow signals). In contrast, we observed no positive endoglin signal in the COS-1 cells transfected with pL-ENG^{L13Q}.

We also performed cell-surface biotinylation for recombinant endoglins expressed in COS-1 cells. In immunoprecipitation-Western blotting, a 90 kDa recombinant endoglin monomer was detected in the wild-type endoglin-expressing cell lysate, but not in the L13Q mutant (Suppl. Fig. 2),

2.5. Distribution of recombinant endoglins

To investigate the intracellular distribution of the recombinant endoglins, we performed immunofluorescence staining for endoglin,

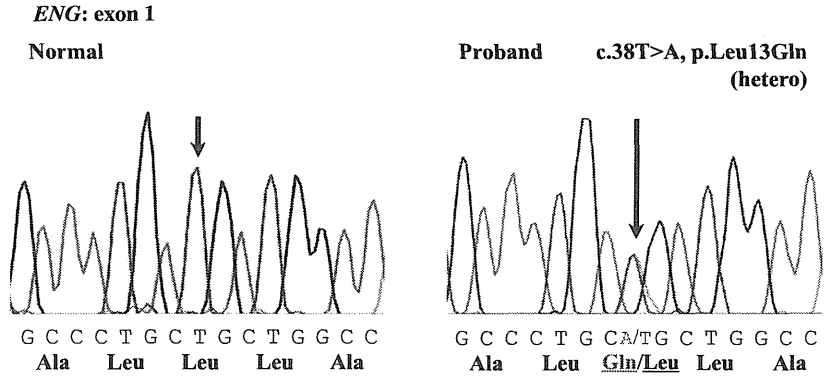

Fig. 1. Detection of c. 38 T>A mutation in endoglin gene. Direct sequencing of *ENG* exon 1 revealed a T-to-A transversion at nucleotide 38. The proband is heterozygous for this transversion, as indicated by a double peak. The same mutation was detected in his sister (data not shown).

together with that for endoplasmic reticulum (ER) by using an antibody against protein disulfide isomerase (PDI) (Fig. 4).

In the COS-1 cells transfected with low amount (0.5 μg) of pL-ENG^{WT}, wild-type endoglin signals were detected in the entire area of the cell and co-localized with ER marker PDI in the peri-nuclear region. Transfection with high amount (5 μg) of pL-ENG^{WT} also showed co-localization of endoglin with PDI, but seemed to cause an ER stress. Meanwhile, in the COS-1 cells transfected with high amount of pL-ENG^{L13Q}, the L13Q mutant endoglin was stained in a scattered pattern and almost never co-localize with PDI. Moreover, PDI staining seemed to be not an ER-stress pattern. We also observed no ER stress pattern in the transfected cells with low amount of pL-ENG^{L13Q}, and no positive green fluorescence signal as well. These results suggested that the mutant endoglin would hardly insert into the ER, leading to severely impaired co-translational processing of the protein.

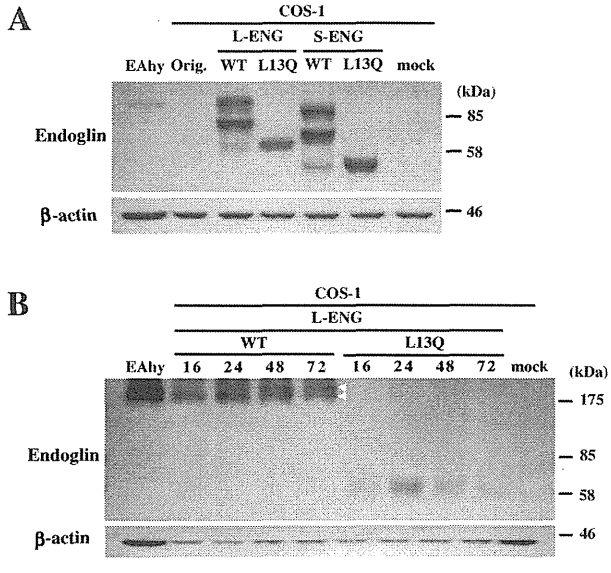

Fig. 2. Comparison of wild-type and Leu13Gln mutant recombinant endoglins. COS-1 cells were transiently transfected with pL-ENG^{WT}, pL-ENG^{L13Q}, pS-ENG^{WT}, or pS-ENG^{L13Q}, and subjected to Western blot analyses. **A:** Western blotting under reducing conditions: After 48 h cell culture, the transfected cells were lysed in SDS sample buffer containing β-mercaptoethanol (β-ME), and subjected to 10% SDS-PAGE followed by Western blotting using anti-endoglin antibody. **B:** Western blot analysis under non-reducing conditions to detect endoglin homodimers: At several time points, the transfected cells were lysed in SDS sample buffer without β-ME, and subjected to 10% SDS-PAGE followed by Western blotting. White arrow-heads indicate two dimerized bands. Whole cell lysates from EAhy926 cells were used as a positive control, and anti-β actin antibody was used as a loading control. Numbers indicate the hours after transfection. Similar results were obtained in three independent experiments.

2.6. Unglycosylated wild-type endoglin showed a similar size to the Leu13Gln mutant

To evaluate the glycosylation of the recombinant endoglins, COS-1 cells were transiently transfected with pL-ENG^{WT} or pL-ENG^{L13Q}, and subsequently treated with a glycosylation inhibitor, tunicamycin. In Western blotting under reduced conditions, tunicamycin treatment decreased the size of recombinant endoglins in the pL-ENG^{WT}-transfected COS-1 cells as well as EAhy926 cells, down to 60 kDa that was a similar size to the L13Q mutant endoglin (Fig. 5). On the other hand, tunicamycin treatment did not affect the size of the recombinant endoglins in the pL-ENG^{L13Q}-transfected COS-1 cells. These data suggested that the largest and second bands could be fully and partially glycosylated proteins, respectively. The third band would be non-glycosylated protein, which was similar in size to the L13Q mutant, suggesting that the L13Q mutant might be impaired in its glycosylation.

2.7. Overexpression of L13Q mutant endoglin in EAhy926 cells showed normal levels of TGF-β-induced Smad signal transduction

Endoglin is a co-receptor of TGF-β receptor complexes and necessary for ALK1 and ALK5 signaling, which induce the phosphorylation of Smad1/5/8 and Smad2/3, respectively, and their nuclear translocation [22,23]. To assess the effects of overexpressed recombinant endoglins on the TGF-β signaling pathway in EAhy926 cells, we analyzed the TGF-β-induced phosphorylation of Smad3. In the untransfected and pL-ENG^{WT}-transfected EAhy926 cells, Smad3 phosphorylation increased with TGF-β1 stimulation for 30 min, although total Smad3 levels substantially unchanged (Suppl. Fig. 3). Smad3 phosphorylation was also up-regulated by TGF-β1 in the pL-ENG^{L13Q}-transfected EAhy926 cells, and the up-regulated level of the Smad3 phosphorylation was almost the same as that in the pL-ENG^{WT}-transfected cells.

3. Discussion

Endoglin is a 180-kDa homodimeric transmembrane glycoprotein primarily associated with the vascular endothelium, and functions as a component of the transforming growth factor-β (TGF-β) receptor complex [24]. Two variants, long- and short-form endoglins, are encoded by a gene (*ENG*) located at 9q33-q34, though the long-form is predominant [7,12,25]. Mutations in *ENG* are responsible for hereditary hemorrhagic telangiectasia type 1 (HHT1), because TGF-β signaling plays a crucial role in angiogenic processes [24,26]. Many mutations have been identified in *ENG* and support the haploinsufficiency model for